UCRL-11374

University of California

Ernest O. Lawrence Radiation Laboratory

THE ELECTRICAL, MAGNETIC, AND OPTICAL PROPERTIES OF SOME COMPLEX ORGANIC SYSTEMS

TWO-WEEK LOAN COPY

This is a Library Circulating Copy which may be borrowed for two weeks. For a personal retention copy, call Tech. Info. Division, Ext. 5545

DISCLAIMER

This document was prepared as an account of work sponsored by the United States Government. While this document is believed to contain correct information, neither the United States Government nor any agency thereof, nor the Regents of the University of California, nor any of their employees, makes any warranty, express or implied, or assumes any legal responsibility for the accuracy, completeness, or usefulness of any information, apparatus, product, or process disclosed, or represents that its use would not infringe privately owned rights. Reference herein to any specific commercial product, process, or service by its trade name, trademark, manufacturer, or otherwise, does not necessarily constitute or imply its endorsement, recommendation, or favoring by the United States Government or any agency thereof, or the Regents of the University of California. The views and opinions of authors expressed herein do not necessarily state or reflect those of the United States Government or any agency thereof or the Regents of the University of California.

UCRL-11374

UNIVERSITY OF CALIFORNIA

Lawrence Radiation Laboratory
Berkeley, California

AEC Contract No. W-7405-eng-48

THE ELECTRICAL, MAGNETIC, AND OPTICAL PROPERTIES OF SOME COMPLEX ORGANIC SYSTEMS

David Frederick Ilten

(Ph. D. Thesis)

May 1964

Reproduced by the Technical Information Division directly from the author's copy.

Printed in USA. Price $2.25. Available from the
Office of Technical Services
U. S. Department of Commerce
Washington 25, D.C.

THE ELECTRICAL, MAGNETIC, AND OPTICAL PROPERTIES OF SOME COMPLEX ORGANIC SYSTEMS

TABLE OF CONTENTS

	Page No.
Abstract	1
I. Introduction - Model Systems in Photosynthesis	3
II. Donor-Acceptor Complexes	4
A. General Introduction - Historical Resume	4
B. The Theory of Mulliken	6
C. Comparisons Between Solution and Solid Complexes	7
III. Charge-Transfer Phenomena in Solids	8
A. Optical Spectroscopy	8
1. Introduction	8
2. Instrumentation	11
B. Photoinduced EPR Signals in Coronene-p-Chloranil Crystals	18
C. Correlation of Conductivity and EPR for o-Chloranil-perylene Complex	18
1. Introduction	18
2. Dark Conductivity	20
3. Calculations	23
4. Heat Treatment	23
5. Results	24
IV. Solution Charge-Transfer Complexes	30
A. A General Search for Photoinduced EPR in Complexes in Solution	30

Page No.

1. Introduction 30
2. Results 30
3. Discussion 33

B. The p-Chloranil-dioxane System 33
1. EPR 33
2. Conductivity 40

C. The Rise and the Decay of Fast EPR Signals 40
1. Introduction 40
2. Results 41
3. The Kinetics of the Rise and the Decay 45
4. Temperature Effects 50
5. Purification Procedures 50

V. Tetrahydrofuran-Tetracyanoethylene Complex 52

A. The Complex 52

B. Photoinduced EPR in the TCNE-THF Complex 52
1. Introduction 52
2. Kinetic Data 54
3. Analysis of the Data 62
a. The Steady State 62
b. The Decay Curve 63
c. The Growth Curve 64
d. Solution of the Kinetic Equation 64
e. Further Analysis of the Results 64
4. Summary 69
5. Experimental 72
a. The Electron Paramagnetic Resonance Spectrometer 72
b. The Light Sources and the Optics 72
c. Materials 73

	Page No.
C. Photoconductivity of TCNE-THF Solution	74
1. Introduction	74
2. Analysis of the Results	74
3. Calculation of Ionic Velocities from Experimental Data	82
4. Calculation of Ionic Velocities from Stokes' Law	83
5. Experimental Technique	84
6. Materials	86
Summary	88
Acknowledgments	90
Appendix I	91
Bibliography	92

THE ELECTRICAL, MAGNETIC, AND OPTICAL PROPERTIES OF SOME COMPLEX ORGANIC SYSTEMS

ABSTRACT

A variety of organic donor-acceptor complexes, both solutions and solids, have been investigated as possible model systems for photosynthetic processes. The aim of the study was to obtain information concerning charge transport and charge separation phenomena in organic materials. The optical dichroism of crystals of coronene-p-chloranil charge-transfer complex was studied. The charge-transfer band was found to be polarized along the needle axis of the crystal--that is, along the line of centers joining the molecules. Photoinduced electron paramagnetic resonance (EPR) signals were observed in the coronene-chloranil complex. Attempts were made to correlate heat-induced EPR signals with heat-induced changes in the electrical conductivity of perylene-o-chloranil crystalline complex. There appeared to be no simple relationship between the two phenomena.

A search for photoinduced EPR signals in liquid complexes was carried out, and a number of systems were found with photosignal rise times of less than one second. The solution most extensively studied was p-chloranil dissolved in dioxane. In this case the rise time for the EPR photosignal was approximately 30 msec. Side reactions, however, complicated the interpretation of the data. The complex formed between tetracyanoethylene (TCNE) and tetrahydrofuran (THF) was not so reactive when irradiated. Also, the free radical produced could be

readily identified from its hyperfine structure to be TCNE negative ion radical. The kinetics for the formation of TCNE negative ion radical by light were studied, and a reaction mechanism was proposed. The data for the photoinduced EPR signals were correlated with data obtained for photoconductivity in the same TCNE-THF system. A kinetic scheme was developed which appeared to be applicable to both the photoconductivity and the photoinduced EPR. The data gave evidence for a reversible photoinduced charge separation in a liquid organic system.

I. INTRODUCTION - MODEL SYSTEMS FOR PHOTOSYNTHESIS

After Calvin's (1) explanation of the biochemical steps of the Carbon Cycle had been proposed, renewed interest was shown in the biochemical problem of primary quantum conversion (2)—how is solar energy converted into chemical potential? The approach to the problem involved the study of the movement of electrons within the molecules composing the photosynthetic apparatus in living organisms. This approach was influenced in part by Szent-Györgyi (3), one of the first to look beneath the levels of cellular and molecular ordering for the explanation of life processes. Evidence was obtained indicating that, once an initial charge separation had taken place, the oxidative and the reductive steps of photosynthesis could proceed independently (4). Presumably the first step in the charge separation is the excitation of an electron by incident radiation. However, the exact nature of the succeeding steps is uncertain.

In the past workers have used a twofold approach to the problem of charge separation in photosynthesis. Besides the direct approach of studying actual photosynthesizing systems, a great deal of effort has been expended in attempting to understand models. It was hoped that studies of model systems could provide information concerning fundamental processes thought to occur in living organisms. Particular attention has been given to charge separation and charge transport phenomena in organic systems. In this laboratory Kearns (5,6) studied electron transfer phenomena in organic solids, with special emphasis on phthalocyanine models for chlorophyll. He discovered that the dark conductivity of phthalocyanine increased greatly when a thin

film of phthalocyanine was doped with a layer of o-chloranil. He proposed that phthalocyanine acted as an electron donor, that o-chloranil acted as an electron acceptor, and that a charge transfer took place between the two molecules. This result suggested that more extensive and general studies of charge-transfer complexes formed between aromatic hydrocarbon donor molecules and quinone acceptor molecules should be carried out.

Eastman (7,8), while continuing work on charge-transfer solid complexes, also studied solutions. One of his aims was to find a solution in which a rapidly reversible transfer of an electron from a donor to an acceptor took place. However, because the systems studied were very reactive, such an electron transfer could not be demonstrated unequivocally to take place. The aim of the present work was to continue studies of model systems for photosynthesis. In so doing, charge separation and charge transport phenomena in both solids and liquids were investigated. In particular, a search for the conditions for the reversible transfer of an electron from a donor to an acceptor molecule in solution was continued. One solution in which a reversible charge transfer appears to take place, from EPR and electrical conductivity data, is the complex formed between TCNE and THF.

II. DONOR-ACCEPTOR COMPLEXES

A. General Introduction - Historical Résumé

If equimolar quantities of o-chloranil (red) and of perylene (yellow) are dissolved in hot 1,2-dichloroethane, a black solution results. Upon cooling, black needles crystallize from the solution. The spectra of both the solution and of the crystals show the absorption peaks of the

constituent compounds, as well as a broad, structureless band not found in either of the components. The original materials may be recovered easily from the solution by column chromatography or from the solid by selective sublimation or by zone refining. This evidence indicates that no irreversible chemical changes take place, and that any association between the component compounds must be weak. These properties are characteristic of the class of intermolecular complexes. The color of such complexes is currently explained on the basis of the charge-transfer or donor-acceptor theory as postulated by Mulliken (9,10,11).

Intermolecular complexes have been known at least since 1844, when Wöhler (12) reported the preparation of quinhydrone, a crystalline complex composed of p-benzoquinone and p-benzosemiquinone in molar proportion of 1:1. In his Lehrbuch of 1866 Kekulé (13) called attention to the theoretical problem posed by the colors of complexes. While p-quinone is yellow and hydroquinone white, the complex, quinhydrone, is metallic green. A gradual accumulation of data for various complexes continued, but it was some time before a satisfactory explanation of their colors was proposed. In 1921 Pfeiffer (14) attempted a systematic classification of organic complexes. The 1927 (15) edition of his book rejected several theories then current and suggested that in the complex the quinone was somehow bound to the unsaturated carbons of the benzenoid component of the complex.

In 1928 Weitz (16) postulated a partially polar bond for complexes. Benesi and Hildebrand (17) were interested in the problem, and in 1948 carried out extensive studies on the complex formed between iodine and

benzene. In 1949 Brackman (18) suggested two resonance forms for the complex, one of which was ionized. Mulliken, adapting Brackman's idea, in 1952 developed a quantum mechanical theory of charge-transfer and applied it to the data of Benesi and Hildebrand. So successful was Mulliken's explanation of the observed colors of donor-acceptor complexes, that it stimulated many new investigations. In recent years a number of review articles (19,20,21,22) have appeared, summarizing both the experimental and the theoretical developments in the field. The most comprehensive of these is Briegleb's Elektronen-Donator-Acceptor-Complexe (23), published forty years after Pfeiffer's original classification of molecular complexes.

B. The Theory of Mulliken

Mulliken presumed that the donor-acceptor complex may be represented by two resonance forms

$$D \ldots A \longleftrightarrow D^{\oplus} \; A^{\ominus} \qquad \text{(II.1)}$$

where D is the donor molecule and A is the acceptor molecule.

D ... A is the resonance form where no charge transfer has taken place, and where the only attractive forces between the molecules are van der Waals forces. $D^{\oplus} \longleftrightarrow A^{\ominus}$ is the resonance form where an electron has been completely transferred from the donor molecule to the acceptor molecule. The ground state of the complex is represented by

$$\psi_N = a\psi_0 + b\psi_1 \qquad \text{(II.2)}$$

ψ_0 = Wave function for the van der Waals structure

ψ_1 = Wave function for charge-transfer structure

where $a \gg b$, and the van der Waals structure predominates.

The excited state is represented by

$$\psi_E = a^*\psi_0 - b^*\psi_1 \qquad \text{(II.3)}$$

where b>>a, and the charge-transfer state predominates.

The charge-transfer absorption is

$$\psi_N \longrightarrow \psi_E \qquad \text{(II.4)}$$

The energy of the charge-transfer absorption is approximately

$$h\nu = E_A - I_D - \frac{e^2}{\varepsilon r_{AB}} \qquad \text{(II.5)}$$

Where

E_A = the electron affinity of the acceptor molecule

I_D = the ionization potential of the donor molecule

$\frac{e^2}{\varepsilon r_{AB}}$ = the coulombic interaction term, and

e = the charge of the electron

r_{AB} = the distance of intermolecular separation

C. Comparisons Between Solution and Solid Complexes

In the solid all of the molecules are complexed, while in solution the following equilibrium exists between the components and the complex

$$D + A \rightleftharpoons \underbrace{D\ldots A \longleftrightarrow D^{\oplus}\ A^{\ominus}}_{\text{COMPLEX}} \qquad \text{(II.6)}$$

Crystalline charge-transfer complexes form interesting structural analogs to photosynthetic systems. The plants exist as alternating layers of carotenoids and chlorophylls, similar to quinone donor and hydrocarbon acceptor laminations in the complexes. The nature of charge separation in solution is not well understood.

III. CHARGE-TRANSFER PHENOMENA IN SOLIDS

A. Optical Spectroscopy

1. Introduction

Optical spectroscopy of charge-transfer crystals was carried out to determine the relationship between the crystal structure and the direction of the charge-transfer transition. In nearly all cases charge-transfer complexes crystallize as long needles. X-ray crystallography has established the structure as alternating layers of donor and acceptor molecules (24). The planes of these layers are oriented at some acute angle to the needle or c-axis of the complex. For example, in the case of quinhydrone (25) the angle is 56 degrees. Although the crystal structure of quinhydrone is well established, the dichroism of the charge-transfer transition is somewhat in doubt. Nakamoto (26) was the first to study the dichroism of charge-transfer crystals. His original microspectroscopy, done in 1952, seemed to indicate that the charge-transfer transition lay perpendicular to the planes of the donor and acceptor molecules. Recently Anex and Parkhurst (27) have done reflection spectroscopy of quinhydrone and have concluded that the charge-transfer transition lies parallel to the needle axis of the crystal, or along the line of centers joining the donor and the acceptor planes.

The charge-transfer band in chloranil-coronene complex is a broad, structureless peak extending from 5000 Å to 6500 Å, with a maximum at approximately 6000 Å. Figure III-1 illustrates the dichroism of the charge-transfer absorption. The data, which were obtained using a microspectrophotometer, showed that the charge-transfer absorption was far more intense when the incident light was polarized parallel to the needle axis of the crystal than when the light was polarized perpendicular to the needle axis. The direction of the needle axis corresponds to the

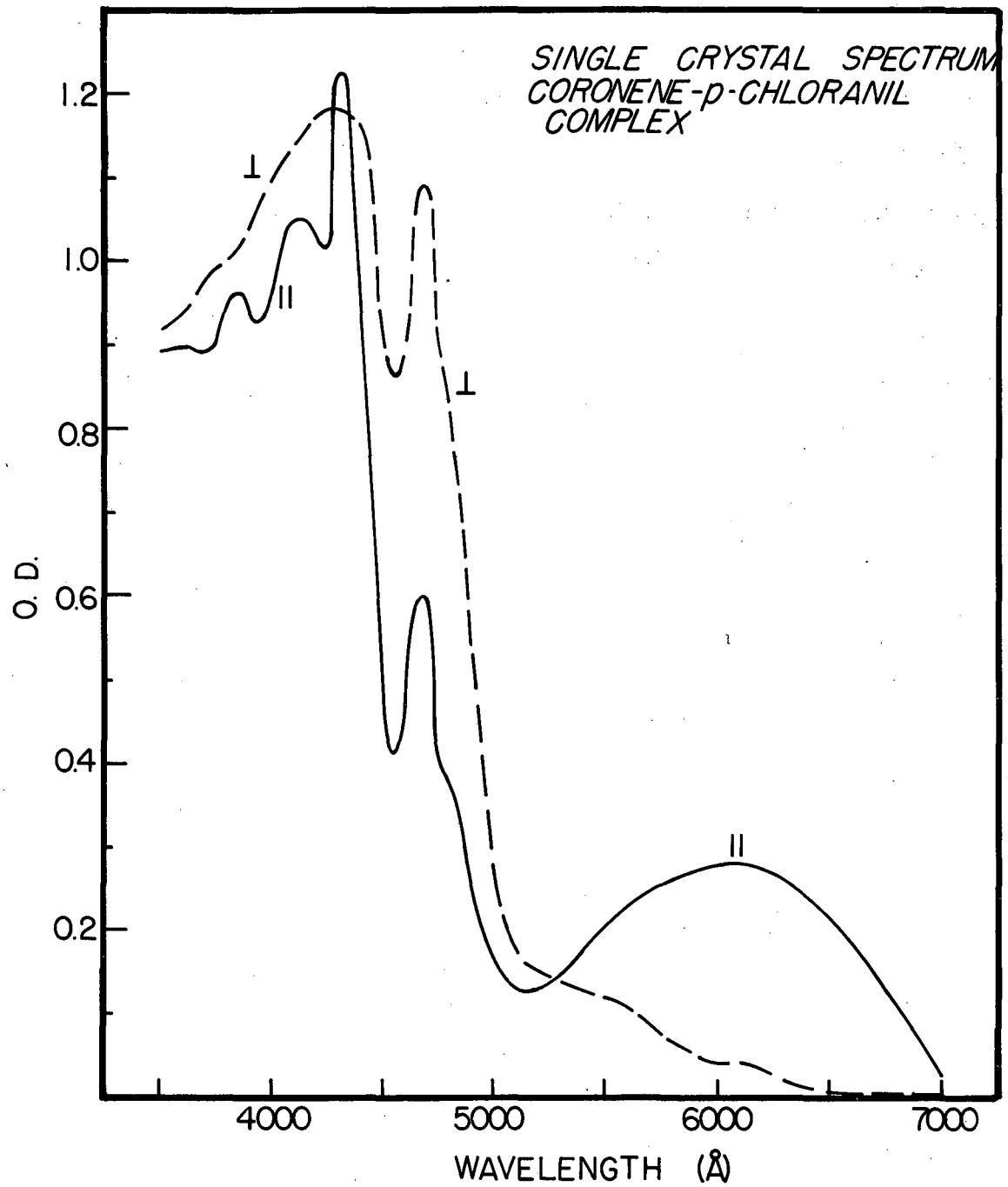

MUB-2247

Fig. III-1. The dichroism of the charge-transfer transition of a coronene-p-chloranil single crystal. ∥ = light polarized parallel to the needle axis of the crystal. ⊥ = light polarized perpendicular to the needle axis of the crystal. The broad, structureless band extending from 5000Å to 7000Å, with a maximum at approximately 6000Å, is the charge-transfer band. The results above indicate that the charge-transfer transition is polarized parallel to the needle axis of the crystal--that is, parallel to the line of centers joining the molecules.

direction of the line of centers drawn between the plane of the donor molecules and the plane of the acceptor molecules (28). Therefore, the charge-transfer transition is polarized along the line of centers between the donors and the acceptors.

This is in agreement with Mulliken's theory (29), which gives the charge-transfer transition moment as

$$\mu = ea^*b(\vec{r}_B - \vec{r}_A) + (aa^* - bb^*)e\,S(\vec{r}_B - \vec{r}_A). \qquad \text{(III.1)}$$

Where the charge-transfer transition is

$$\psi_N = a\psi_0 + b\psi_1 \longrightarrow \psi_E = a^*\psi_0 - b^*\psi_1 \qquad \text{(III.2)}$$

and a and b are normalized so that

$$a^2 + 2abS + b^2 = 1, \qquad \text{(III.3)}$$

where

e = the charge on the electron,

r_A and r_B are the average positions of the electron in the B or A orbitals, respectively,

S = the overlap integral between ψ_0 and $\psi_1 = \int \psi_0\psi_1\, dv$

* denotes the excited state.

The first term of Equation (III.1) represents the transition moment along the line of centers between the molecules. According to Mulliken, the second term of the equation is in general small. This results from the small overlap integral, S, for charge-transfer complexes.

The crystals studied were grown from a solution of coronene and chloranil in hot 1,2-dichloroethane. Many of the samples were too optically dense to be suitable for microspectroscopy. However, certain of the needles crystallized from the mixed solution had almost exactly the density of coronene itself. Also, the crystal structure was very

nearly that of coronene. However, the crystals had the intense greenish color which is characteristic of the complex. This indicated that, although the crystals were essentially coronene, they had sufficient chloranil impurities so that the crystals were, in effect, a dilute solution of the complex in a coronene host. The crystal structure of coronene (28) is shown in Figure III-2. Figures III-3 and III-4 give the solid state spectra of coronene and of the complex. Figure III-5 shows the spectrum of the complex in 1,2-dichloroethane.

2. Instrumentation

The microspectrophotometer was a prototype instrument designed and constructed by the Applied Physics Corporation, Monrovia, California, for use with the Cary Model 11 Spectrophotometer. A block diagram of the instrument is shown in Figure III-6. The instrument can be used either as a microscope or as a recording spectrophotometer. It is patterned after a device constructed originally by Tsuchida and Kobayashi (30). Light from a microscope lamp is focused by a condensing lens onto the sample on a glass slide, from which it passes through an objective lens. When a mirror is inserted at this point, the beam is deflected to an eyepiece. The numerical aperture of the condensing lens is 0.56, and the total magnification obtained from the lenses and eyepiece is 300 diameters. Crystals were placed on the slide and a specimen of suitable transparency for spectral work was selected visually. When the microscope lamp is turned off and the deflecting mirror moved out of position, the instrument can function as a spectrophotometer. For this work the tungsten lamp normally provided with the spectrophotometer was replaced with a General Electric 1955 lamp operated at 28 volts and 150 watts. The lamp is a small source operated at a high temperature. It is

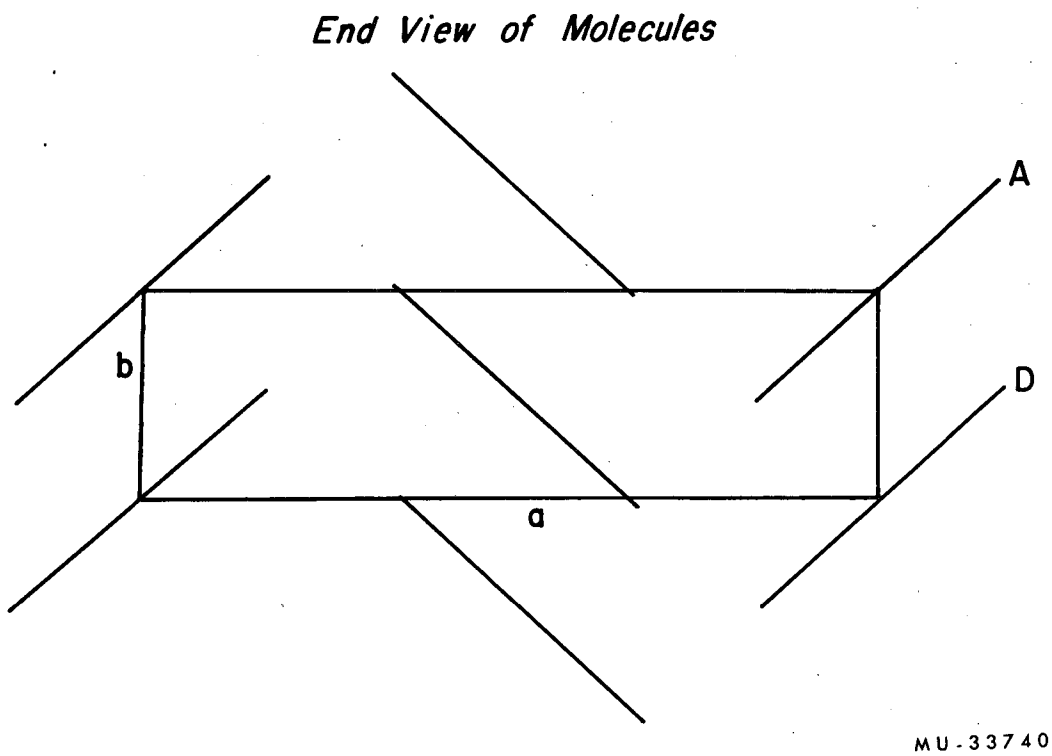

Fig. III-2. The crystal structure of coronene [after Robertson (28)]. D and A denote the position of the donor and the acceptor molecules, respectively, in the case where chloranil has partially displaced coronene in the coronene crystal lattice and resulted in the formation of a charge-transfer complex.

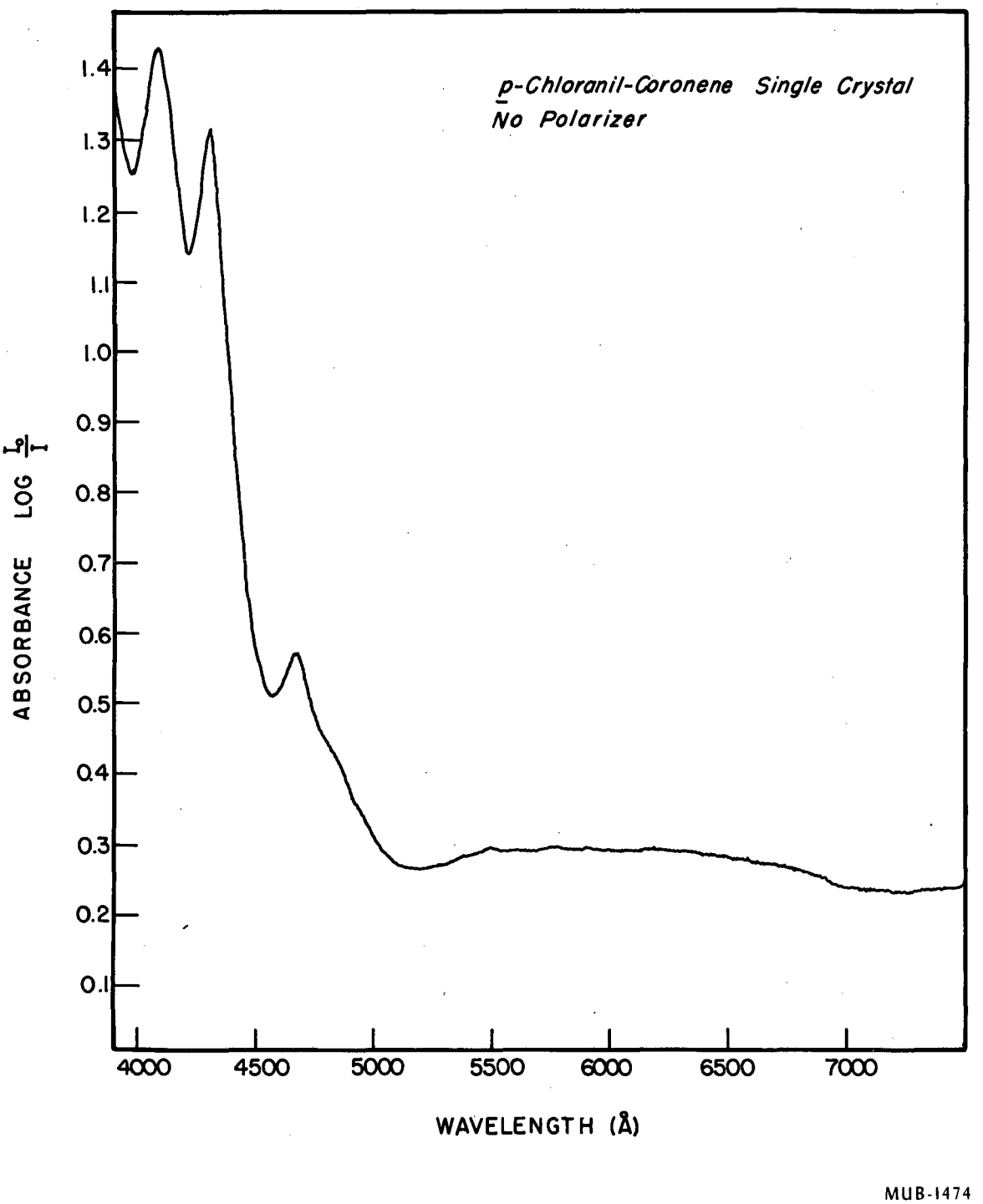

Fig. III-3. Optical spectrum of p-chloranil-coronene complex taken with Cary 11 spectrophotometer with microscope attachment. (Base line corrections have been made.)

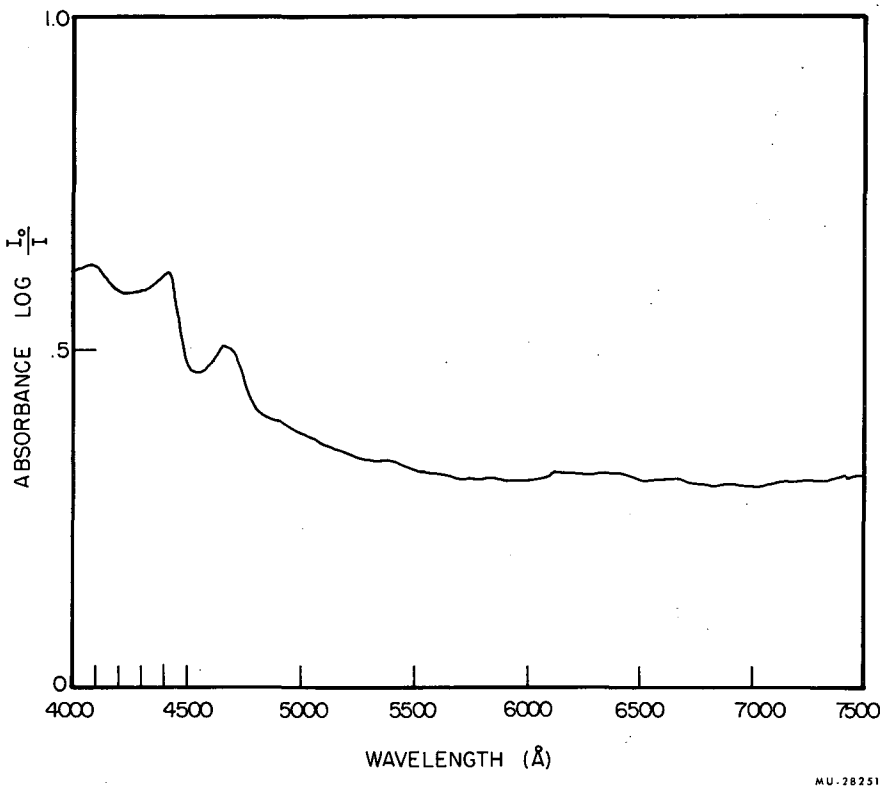

Fig. III-4. Coronene with polarizer perpendicular to needle axis of crystal.

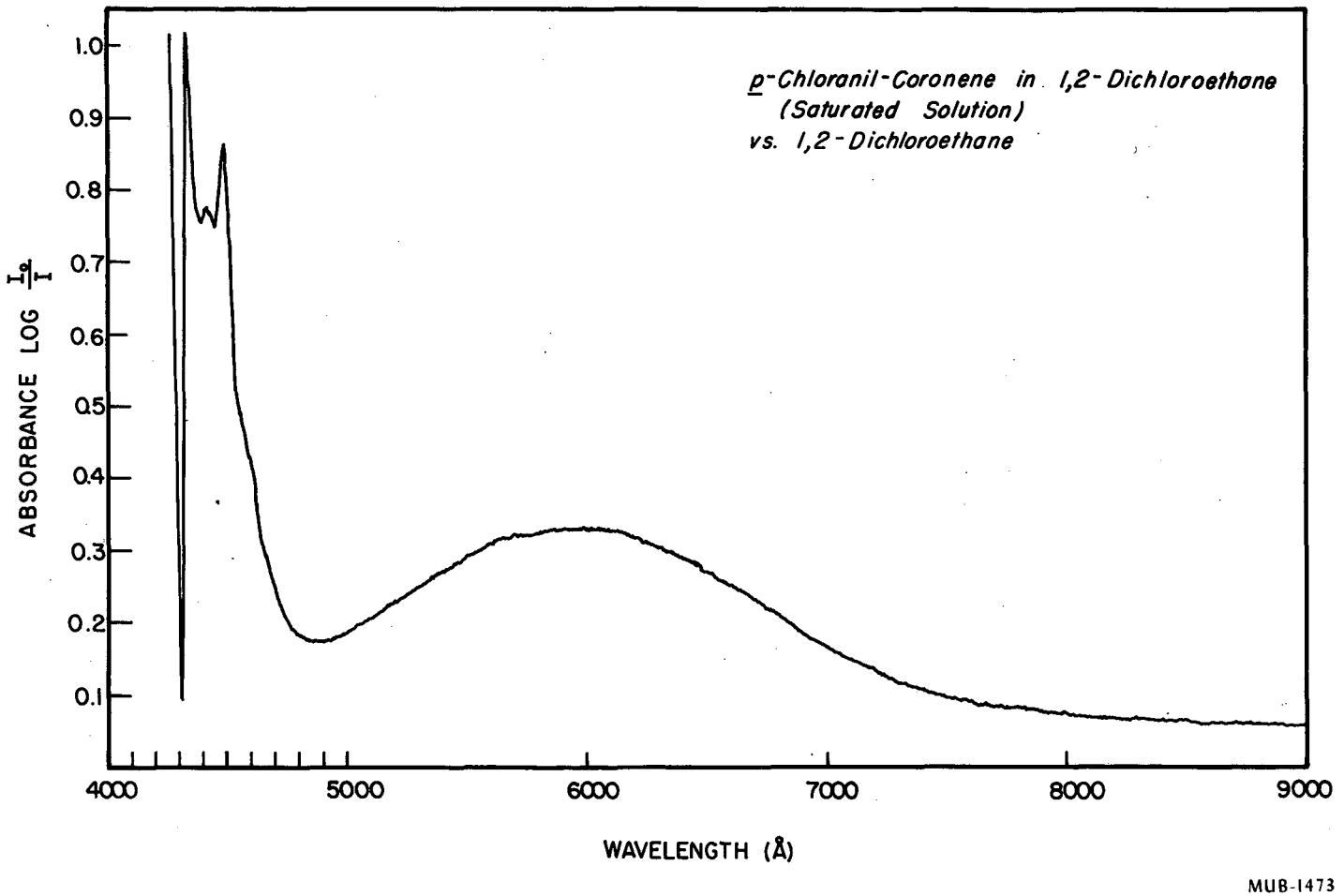

Fig. III-5. Spectrum of p-chloranil-coronene complex in 1,2-dichloroethane showing the charge-transfer band.

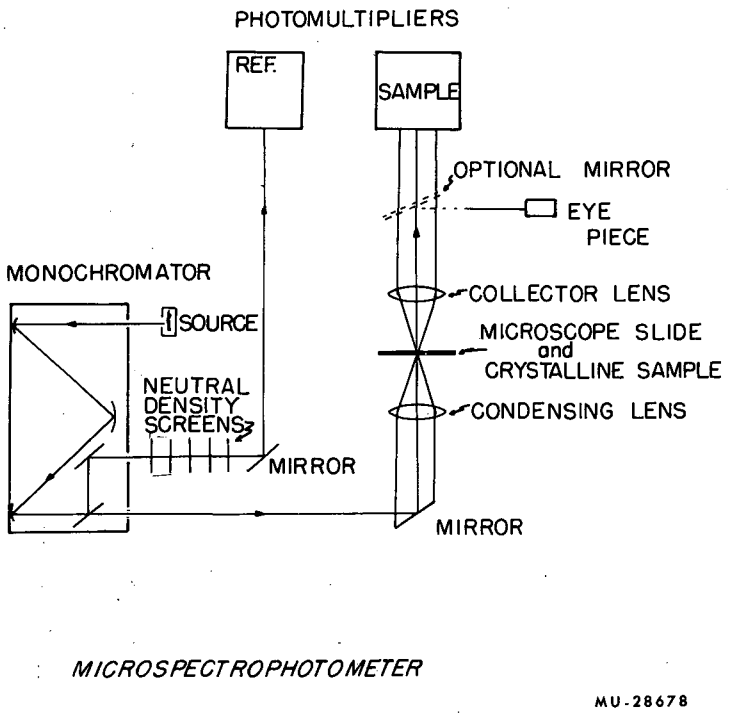

Fig. III-6. Microspectrophotometer.

enclosed in a quartz sheath and employs a tungsten-iodine cycle to reduce deposits on the sheath. The beam from this source passes through the monochromator and is then split into a reference beam and a sample beam. The spectrophotometer is a double beam type, which uses two photomultipliers to determine the ratio of the intensities of the reference and the sample beams. The sample beam passes from the monochromator through one of a set of apertures, such that the field illuminated on the microscope slide has a diameter of 12, 20, or 80 microns. The sample beam is then reflected from a front face mirror and focused by the condensing lens onto the crystal on the microscope slide. An objective lens collimates the sample beam, the intensity of which is measured by one photomultiplier. Before the reference beam passes to the second photomultiplier for detection, its intensity can be matched approximately to the intensity coming from the aperture by using any combination of five neutral density screens provided with the instrument. The 1P28 photomultipliers originally supplied with the spectrophotometer were replaced with HTV-R136 photomultipliers (Applied Physics Corporation, Monrovia, California), which have a high sensitivity at wavelengths in the red. Because reflecting optics are used throughout, the microscope is completely achromatic. It has been possible to obtain solid state spectra over the range from 3500 Å to 7500 Å for a sample somewhat larger than 20 microns in diameter.

In each case illustrated, base line corrections have been made and the spectrum replotted. Crystals which appeared reasonably smooth and transparent when viewed through the microscope eyepiece were selected for spectroscopic work. The dichroism of the charge-transfer transition was shown by inserting a polarizer (Polaroid, Type HN38) in the sample beam and orienting it either parallel or perpendicular to the long needle axis of the crystalline complex.

B. Photoinduced EPR Signals in Coronene-p-Chloranil Crystals

Coronene-p-chloranil complex crystallized from 1,2-dichloroethane solution showed a small EPR signal (approximately 10^{15} spins/gm). The spin concentration could be increased by irradiating the crystals with light from a tungsten source. The concentration of unpaired electrons increased as the light intensity was increased—until a maximum level was reached. From that point, further increases in intensity resulted in a decreasing spin concentration. The spin level decayed slowly to its original value after the light was shut off. Raising the temperature to 80° increased both the spin concentration in the dark and the spin photosignal. Also, the maximum of the signal level vs. light intensity curve occurred at a lower light intensity at 80° than at room temperature.

As is explained in the next section, Eastman assumed that imperfections, either trapped free radicals or lattice defects, are responsible for the observed paramagnetism. Heating the crystals produces such imperfections. The photoinduced EPR may be explained by considering the electrons to be excited into an excited state where they are unpaired. Once the maximum number of levels have been singly filled, further excitation results in the pairing of electrons in the excited state and a decrease in the observed spin concentration. Heating the crystals populates the upper levels and decreases the intensity of light at which pairing begins.

C. Correlation of Conductivity and EPR for o-chloranil-perylene Complex

1. Introduction

In 1954 Akamatu, Inokuchi, and Matsunaga (31) at the University of Tokyo observed paramagnetism in solid complexes formed between hydro-

carbons and halogens. Also, in that same year Kainer, Bijl, and Rose-Innes (32) found electron paramagnetic resonance signals in arylamine-quinone solids. In 1961 Eastman (33) reported the results of extensive studies on the paramagnetism of charge-transfer solids formed between polycyclic aromatic hydrocarbon electron donors and tetrahalogenated quinone acceptors. He found that it was possible, under proper conditions, to grow crystals of certain complexes which were actually spin-free. However, paramagnetism could be induced in the crystals by heating. Comparing these results with the work of several other investigators, Eastman concluded that the paramagnetism observed was attributable to imperfections in the crystal lattice. The term "imperfections" was defined to include either trapped free radicals or crystalline defects.

The heat-induced changes in the EPR signal suggested that changes in electrical conductivity might result from heat treatment as well. Crystals of o-chloranil-perylene complex were prepared by dissolving equimolar quantities of the components in boiling 1,2-dichloroethane and allowing the resulting solution to cool. EPR data showed the room-temperature concentration of unpaired electrons in the freshly prepared solid complex to be $< 10^{16}$/gm. However, when the complex was heated at 60° for an hour and then cooled to room temperature, there was a decided irreversible increase in the concentration of unpaired electrons. The spin concentration continued to increase as a function of heating time until a maximum level was reached. From that point there was a gradual decrease in the concentration of unpaired electrons with further heating. Dark conductivity measurements were made on samples of o-chloranil and perylene, and on the complex. Samples of the complex for both conductivity and EPR measurements were prepared and heated simultaneously for various periods of time so that changes in these properties could

be correlated. Table III-I and Figure III-7 indicate the results.

2. Dark Conductivity

[Electrical conductivity measuring techniques for organic materials have been summarized by Inokuchi (34).]

Dark conductivity was measured on samples of the materials that had been pulverized and then pressed into pellets approximately 1.5 cm in diameter and 0.1 cm thick. These were prepared by placing the powdered sample into a die, evacuating to remove moisture, and then applying 25,000-lb force for at least 2 minutes. This was equivalent to a pelleting pressure of 125,000 psi. The conductivity apparatus was a slightly modified version of that described by Kearns (35). The samples were placed between two steel cylinders and surrounded by a glass cylinder. Platinum discs in contact with the ends of the steel cylinders served as electrodes for connecting the sample into the measuring circuit. The resistance was determined by using a standard 10-ohm resistor which was placed in series with the sample and a dc source of 17.5 volts. The sample, cylinders, and electrodes were enclosed in a brass chamber which could be evacuated. The temperature of the system was controlled by circulating a methanol-water mixture from a thermostat bath through coils surrounding the chamber. A copper-constantin thermocouple, fitted into the chamber through a Radiation Laboratory Seal and an epoxy plug, was used for temperature determinations. A pressure of approximately 100 kg/cm^2 was applied to the sample by a lever arm. As the conductivity was greatly changed if air were present in the system, all measurements were carried out at 10 mm pressure. The high volatility of the materials made it more difficult to obtain low pressures under conditions of even moderate temperature.

TABLE III-I

Activation energies and ESR measurements

Substance	Activation energy of conduction, ΔE, (ev)	Concentration per gram of unpaired electrons (at room temperature)
o-chloranil	2.42 ± 5%	
perylene	0.55 (0.98[a]) 1.00[c]	
complex (unheated)		$< 1 \times 10^{16}$
complex (heated, 1 hr)		4.8×10^{17}
complex (heated, 2 hr)		1.0×10^{18}
complex (heated, 3 hr)		3.3×10^{18}
complex (heated, 4 hr)	0.25 (0.05 ± 15%[b])	

[a]Value for sublimed film: D. C. Northrop and O. Simpson, Proc. Roy. Soc. (London) A234, 124 (1956).

[b]ESR value which may be the ΔE for a phenomenon unrelated to the conductivity.

[c] H. Inokuchi (34) Thin film measurement

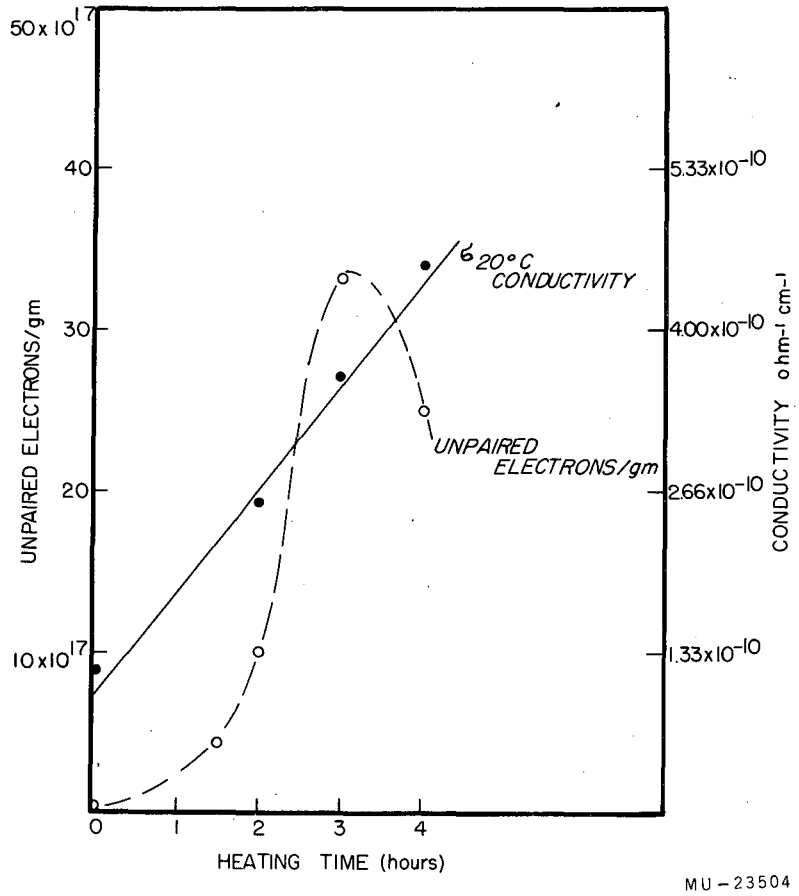

Fig. III-7. Comparison of changes in conductivity and number of unpaired electrons per g (for o-chloranil-perylene as a function of heating time.)

3. Calculations

The dark conductivity was measured for o-chloranil, perylene, and the complex. The resistivity of the sample, ρ, in ohm-cm was computed as

$$\rho = AR/d \qquad \text{(III.4)}$$

where

R = the measured resistance (in ohms),

A = the area of the sample (in cm^2),

d = the thickness of the sample (in cm).

The activation energy of conduction for these substances were determined by plotting resistivity, ρ, vs. $(\text{temperature})^{-1}$. Then

$$\Delta E = 2.303\ mk \quad \text{or} \quad \Delta E = 1.99 \times 10^{-4}\ (\text{in eV}) \qquad \text{(III.5)}$$

where

E = the activation energy for conduction (in electron volts),

k = Boltzmann's constant = 8.63×10^{-5} eV,

m = the slope of the semilog plot.

This calculation was based on the assumption that the activation energy for conduction followed the Boltzmann Relation

$$\rho = \rho_o e^{\Delta E/kT} \quad \text{or} \quad \sigma = \sigma_o e^{-\Delta E/kT}. \qquad \text{(III.6)}$$

4. Heat Treatment

Pellets of the complex were pressed as described previously and then placed into sample tubes. These tubes were evacuated to 10^{-4} Torr pressure and then filled with nitrogen. One pellet was powdered and 0.025 gm of the resulting powder was placed into each of five EPR tubes. These, also, were evacuated and then filled with nitrogen. Four EPR and four conductivity tubes were placed into an oil bath that was

maintained at 85 ± 4°. Samples were removed after one-hour intervals and cooled in an ice bath to prevent further reaction. The EPR and conductivity of these samples were then measured. The temperature dependence of these properties was determined for the sample that had been heated four hours.

5. Results

As illustrated in Figures III-8 and III-9, a plot of the log of resistivity vs. the reciprocal of the temperature gave the expected linear relationship over the temperature range investigated for the o-chloranil and the perylene. This was true, also, for the complex up to about 60°, at which temperature there was a deviation, probably indicating the onset of further heat-produced changes in the sample. The data in Figure III-7 indicate that although both the spin concentration and the conductivity are increased by heat treatment, the two phenomena do not follow the same kinetics. The conductivity increased linearly with heating time or

$$d\sigma/dt = k. \qquad \text{(III.7)}$$

This, in turn, means that the concentration and the mobility, μ, of the charge carriers were increasing in such a fashion that

$$d(n\mu)/dt = k. \qquad \text{(III.8)}$$

Also, the activation energy for conductivity decreased a factor of two in four hours of heating. On the other hand, the spin concentration increased as some power of the heating time reached a maximum, and decreased. The conductivity increased a factor of four in four hours of heating, while the spin concentration increased several orders of magnitude. The activation energy for conduction was approximately five times as great (Fig. III-10) as the activation energy as

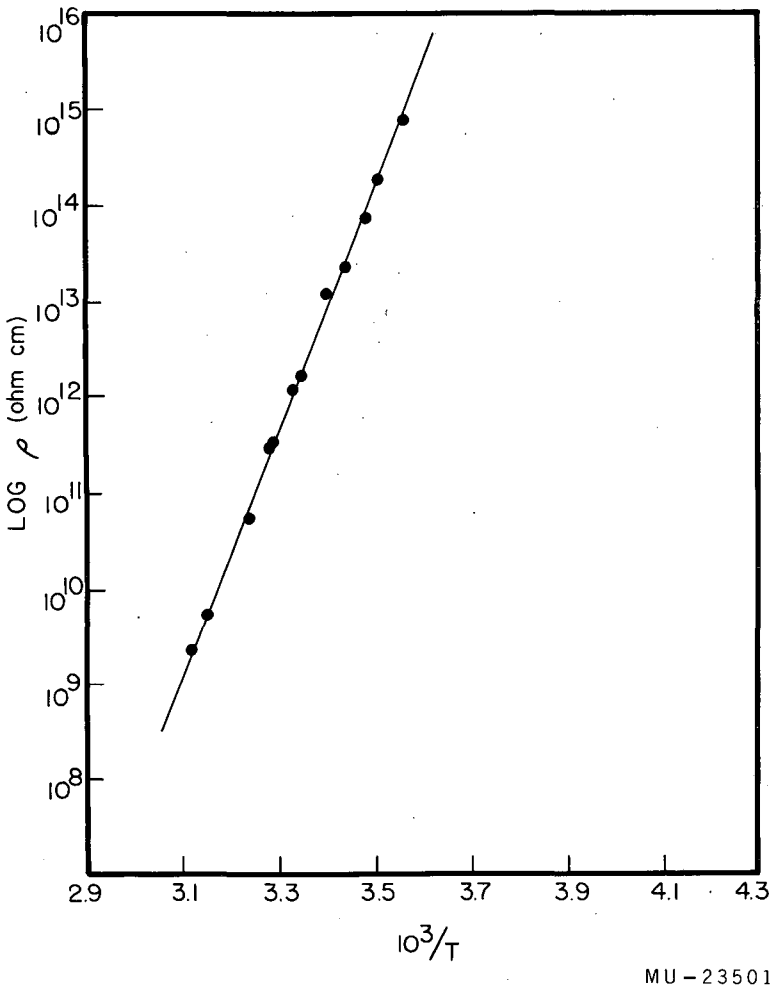

Fig. III-8. Log resistivity vs (temperature)$^{-1}$ for a pellet of o-chloranil.

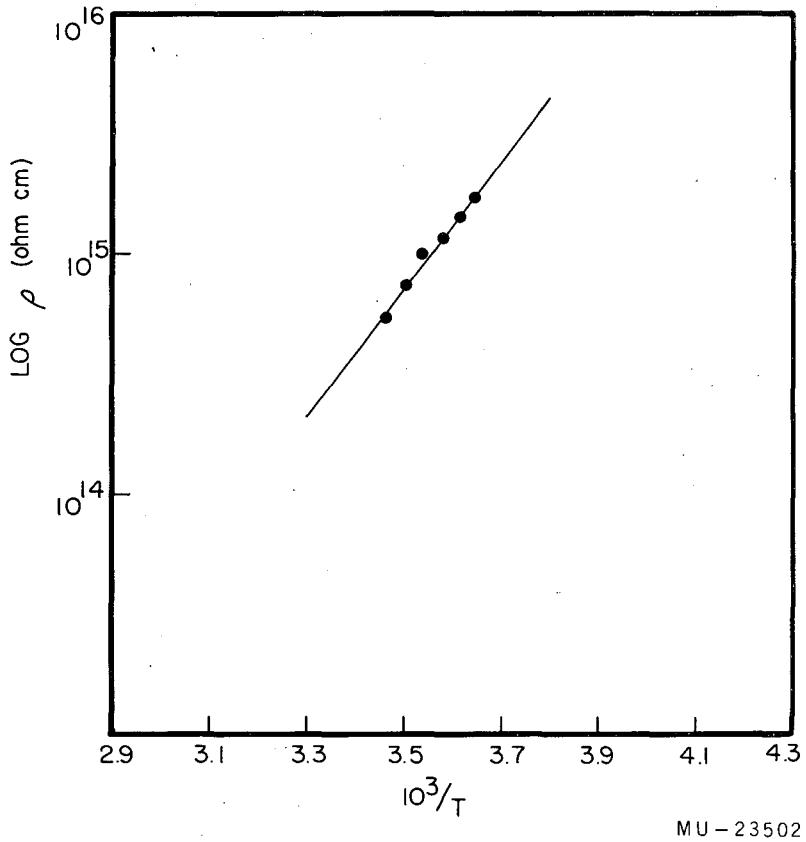

Fig. III-9. Log resistivity vs (temperature)$^{-1}$ for pellet of perylene, 0.08 cm thick, 1.29 cm in diameter.

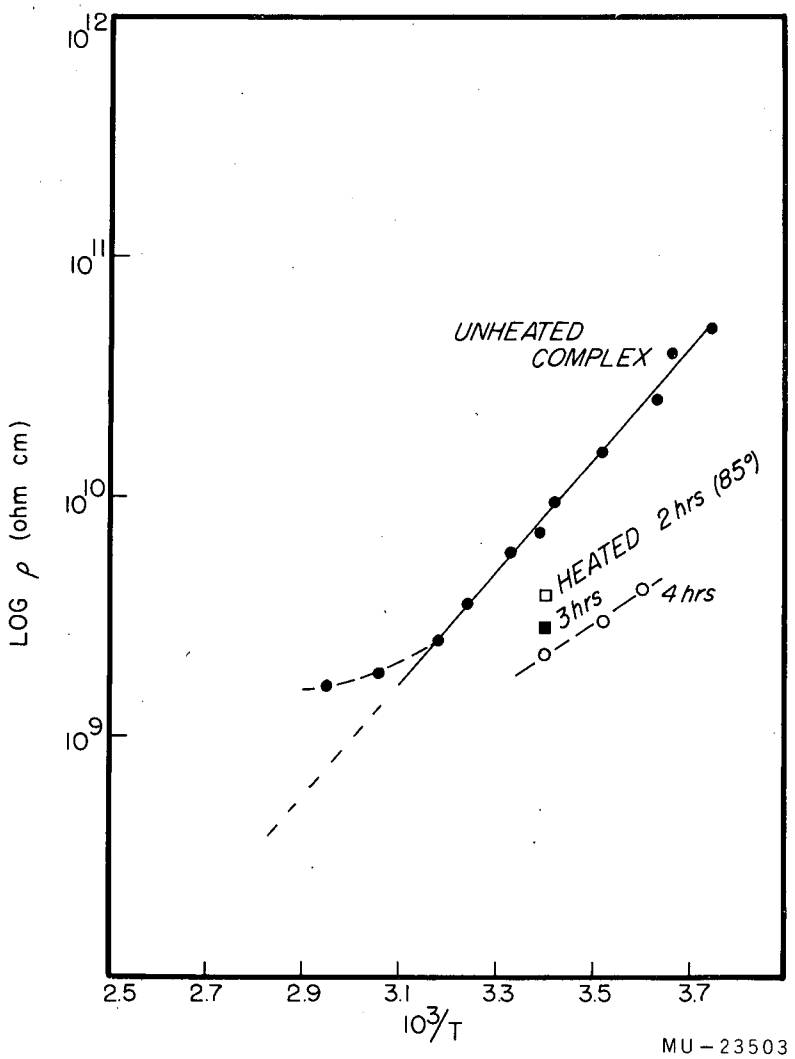

Fig. III-10. Log resistivity as a function of temperature for heated and unheated complexes of o-chloranil and perylene.

determined by EPR (Fig. III-11). Thus, the attempts to correlate EPR with electrical conductivity did not give a readily apparent, simple agreement.

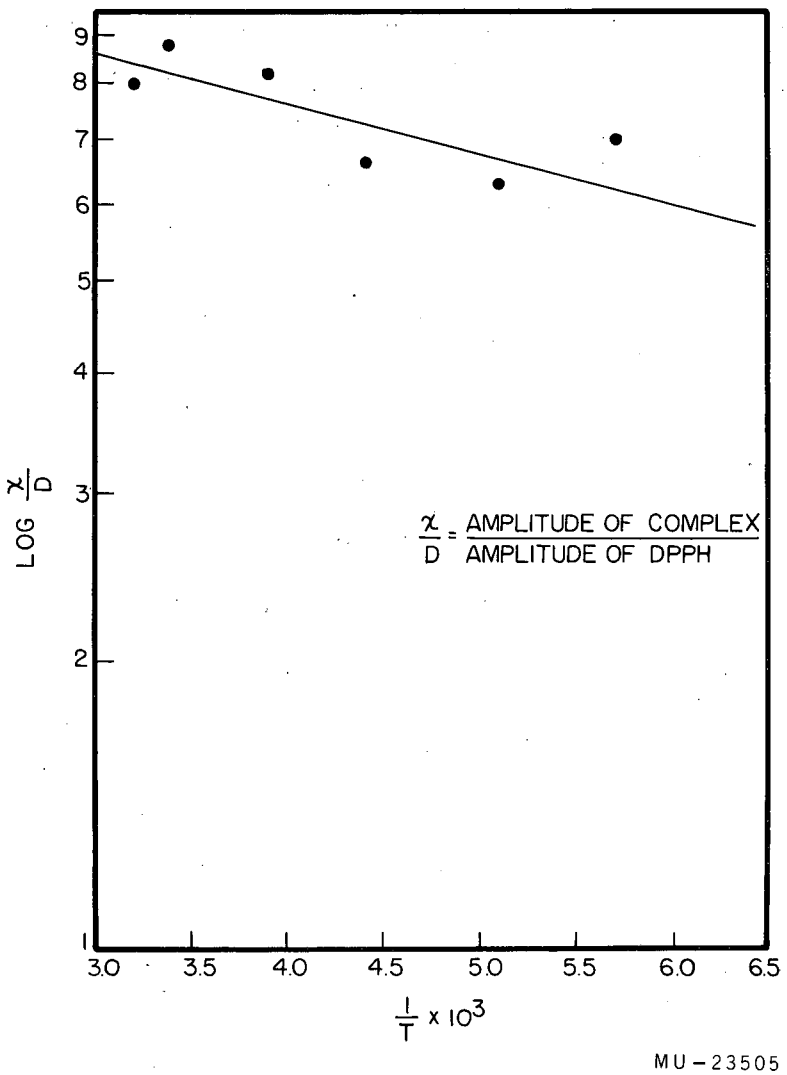

Fig. III-11. Temperature dependence of ESR for solid complex of o-chloranil and perylene. (DPPH = diphenylpicrylhydrazyl.)

IV. SOLUTION CHARGE-TRANSFER COMPLEXES

A. A General Search for Photoinduced EPR in Complexes in Solution

1. Introduction

Solution charge-transfer complexes were investigated in hopes of observing photoinduced changes in their electrical and their magnetic properties. This aspect of the study of model systems for photosynthesis was given impetus by the work of Lagercrantz and Yhland (36,37,38), who in 1962 reported having produced EPR photosignals in a solution of p-chloranil in tetrahydrofuran (THF). They attributed the signals to the unpairing of the electrons involved in the formation of a charge-transfer complex between the donor (THF) and the acceptor (chloranil). The signals were approximately 15 gauss wide, had g-values of very nearly 2, and exhibited rise and decay times of less than one second, the instrumental time constant. If, in fact, the photosignals were caused by free electrons excited to the charge-transfer level of the complex, the solutions might be expected to show very interesting electrical properties, such as photoconductivity. The present investigation, therefore, had a threefold purpose: to study various complexes which might show EPR photosignals, to obtain better measurements of the rise and decay times of the signals, and to correlate the EPR data with electrical conductivity measurements.

2. Results

The results of preliminary attempts to observe EPR photosignals in a number of donor-acceptor systems are summarized in Table IV-I. For these investigations solvents were distilled at least once and the solutes were recrystallized. The EPR data were obtained using the spectrometer described under Section V.B.5a. The samples were first tested for dark

TABLE IV-I

(0.05 M solutions of p-chloranil were prepared in the following solvents)

A.

Solvents	Color of Solution	Results (signals ca. 15 gauss wide)
Benzene	Yellow	No dark signal, no light signal
p-Xylene	Orange (Yellow)	No dark signal, possible light signal
Mesitylene	Orange (Yellow)	No dark signal, small light signal
Phenitol	Red (Orange)	No signal
o-Chlorophenol	Orange (Red)	No dark signal, small light signal, rapid rise and decay time (<1/10 sec)
α-Chloronaphthalene	Red (Orange)	No dark signal, no light signal
Pyridine	Dark solution (Precipitate)	No dark signal, no light signal
Quinoline	Dark solution (Some precipitate)	Very large dark signal, no fine structure. No appreciable enhancement in light (ca. 10^{18} spins/ml)
Tetrahydrofuran	Yellow	No dark signal, small light signal (ca. 10^{15} spins/ml)
Thiophene	Orange	No signal
p-Dioxane	Yellow (Green)	No dark signal, large light signal (ca. 10^{17} spins/ml). Slow response enhancement when light turned off
Morpholine	Reddish-brown	Small dark signal, factor of 10 increase in light, enhancement when light off
Piperidine	Reddish-brown	No dark signal, small light signal, rapid response
1,2-Dimethoxyethane	Yellow	No dark signal, small light signal, rapid response
Nujol (< 0.05 M)	Yellow solution	No dark signal, small light signal, long lived
Triphenyl Phosphite	Orange-red	No signal

TABLE IV-I (Continued)

B. Other Systems

Compound	Color of Solution	Results (signals ca. 15 gauss wide)
o-Chloranil + Thiophene (0.05 M)	Orange-red	No dark signal, small light signal ca. 30 gauss wide
o-Chloranil + Diphenyl-ether (0.05 M)	Reddish	No dark signal, small light signal
TCNE* + Diphenylether (0.05 M)	Reddish	No dark signal, small light signal
TCNE + Pyridine	Dark brownish soln.	Dark signal; 9-line hyperfine structure
TCNE (0.05 M) Pyridine (0.5 M) $EtCl_2$ Solvent	Dark brownish soln.	Dark signal; 9-line hyperfine structure
Perylene (0.001 M) + hexafluorobenzene	Yellow-green	No dark signal, small light signal

TCNE* = tetracyanoethylene

signals by placing 0.2 ml of the material into quartz tubes of 4-mm outside diameter. The tubes were evacuated and then placed into the Varian 4531 rectangular cavity of the EPR spectrometer. A General Electric AH-6 high pressure mercury lamp, 70 cm away, was focused onto the slots of the cavity by means of a pyrex lens located 15 cm from the cavity. A Corning 0-52 (7380) filter having transmission values of 20% at 350 mμ, 50% at 360 mμ, and 90% at 400 mμ was inserted between the light source and the sample.

3. Discussion

As indicated by the results tabulated in Table IV-I, the systems investigated showed widely differing spin concentrations, rise times, and decay times. This certainly indicated that a variety of processes were taking place. The cases where the rise times and the decay times were short may truly result from electronic processes, although the instrumental response time was too long for this to be verified in the preliminary studies. The systems with long rise times and decay times may involve an electron transfer as an initial process, but this initial electron transfer is undoubtedly followed by a "chemical" process, such as the abstraction of a hydrogen atom from the donor.

B. The p-Chloranil-dioxane System

1. EPR

One of the systems studied in more detail was p-chloranil dissolved in p-dioxane. The dioxane was twice distilled and then dried by refluxing over sodium and distilling. The p-chloranil was obtained from K and K Laboratories in Jamaica, N. Y., and was recrystallized from benzene as yellow needles approximately 2 cm long. A 0.05 M

solution of p-chloranil in p-dioxane was prepared and then degassed by 8 freeze-pump-thaw cycles. The samples showed no EPR signal in the dark. However, large signals were observed when the solutions were irradiated. The growth curve for these is shown in Figure IV-1. It will be noted that the rise to maximum spin concentration was not instantaneous, but required approximately 1-1/2 min—far too long for a simple electron transfer process. The decay was, likewise, a slow process, and is shown in Figure IV-2.

The decay curve may be analyzed kinetically as in Figures IV-3 and IV-4. In Figure IV-3 the reciprocal of the spin concentration is plotted against time. If second order decay kinetics were followed, this would be expected to give a straight line. There appears to be a good deal of departure from linearity. In Figure IV-4 the log of the photosignal is plotted against time, giving a curve that can be analyzed into two straight lines. This result seems to indicate the existence of two independently decaying paramagnetic species, having half lives of 0.75 min and 9 min, respectively.

The curve shown in Figure IV-5 illustrates a peculiar light reaction occurring in a solution of p-chloranil in dioxane which had been irradiated for about 10 min. When the light was cut off with a shutter, there was an initial small increase in the signal level, which was followed by a gradual decrease in the signal level. Irradiation of the sample once more resulted in a rapid decrease in signal level, followed by a gradual increase. Repeating the cycle showed an even more pronounced increase in the spin concentration when the light was cut off. These facts seemed to indicate that at least two competing photoinduced processes were taking place, one producing spins, and the other causing

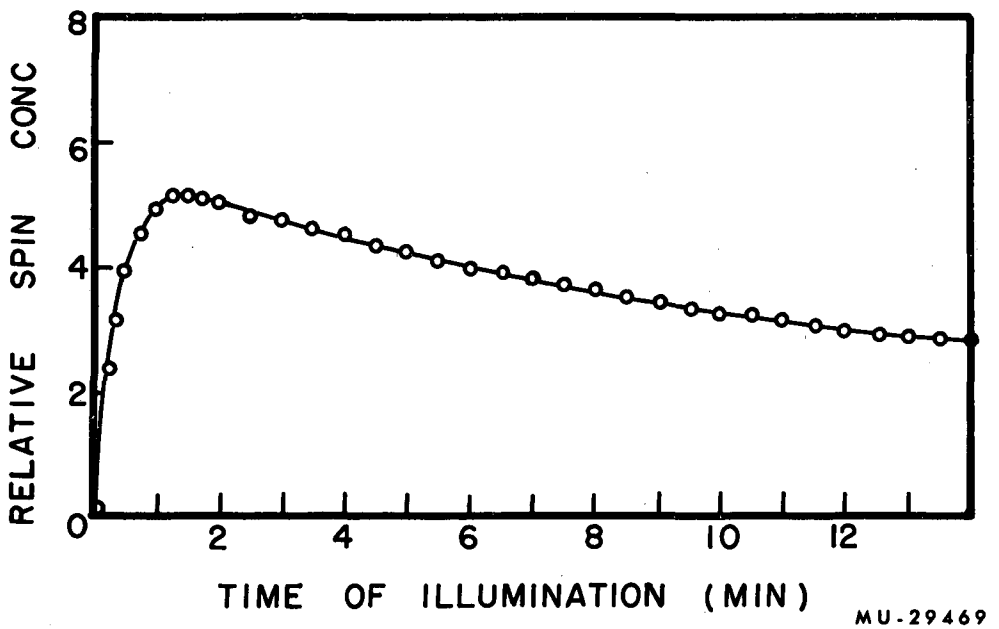

Fig. IV-1. Photoinduced EPR signal in 0.05 M solution of p-chloranil in dioxane.

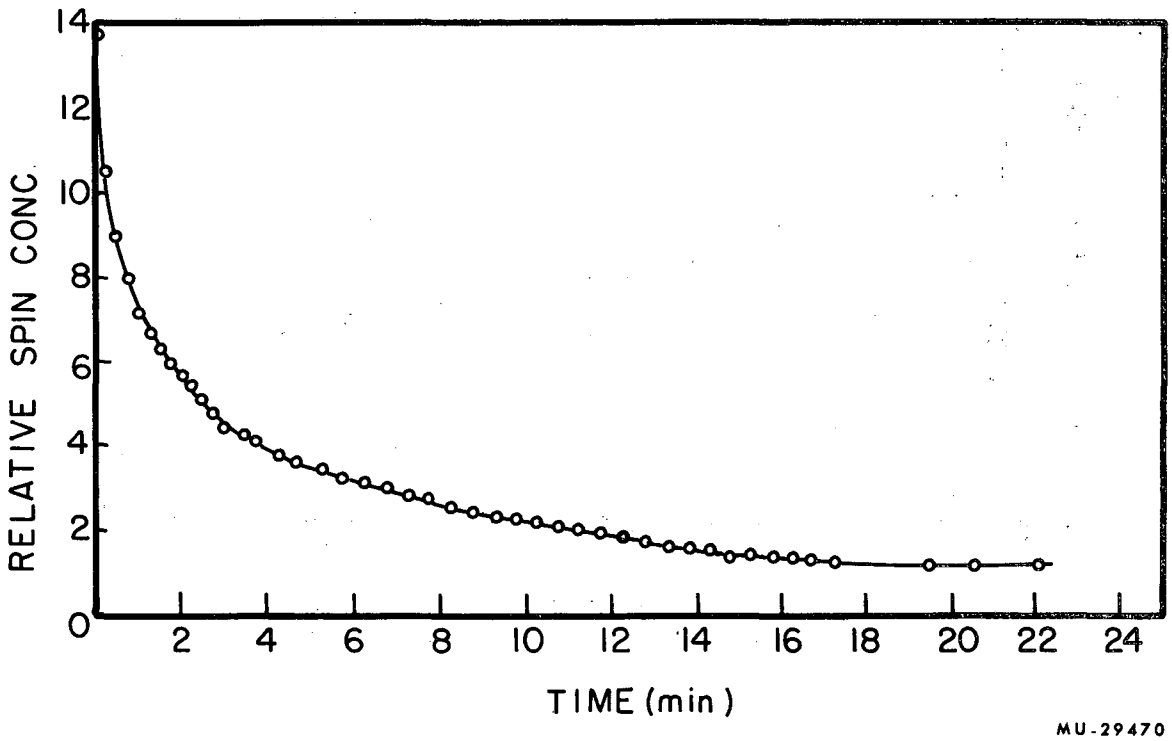

Fig. IV-2. Decay of photoinduced EPR signal in 0.05 M solution of p-chloranil in dioxane.

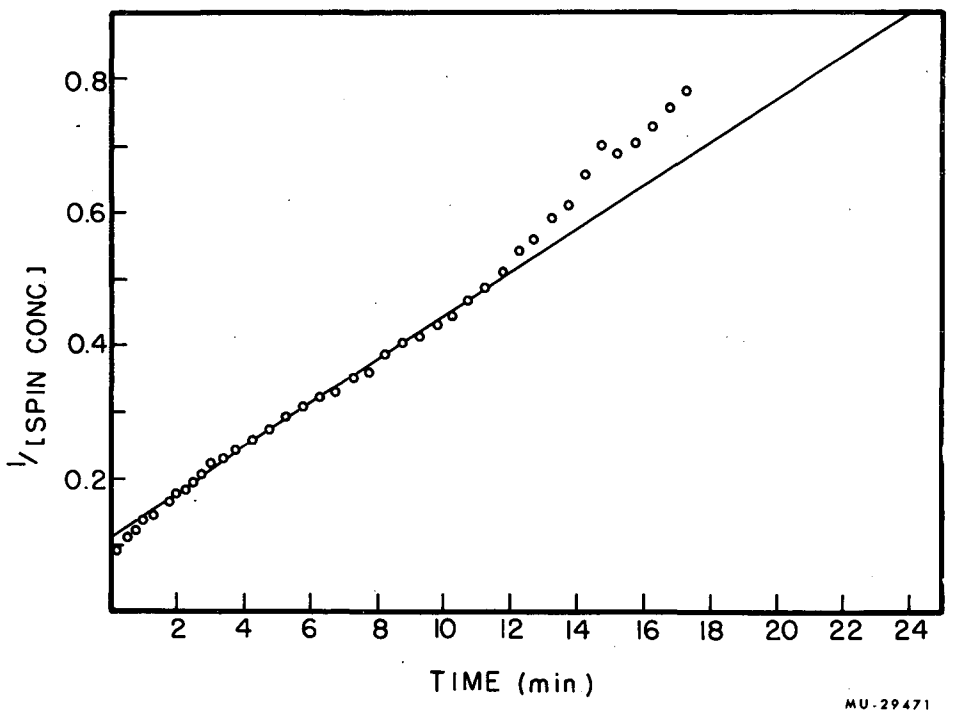

Fig. IV-3. Decay of photoinduced EPR signal in solution of 0.05 M p-chloranil in dioxane. The reciprocal of the spin concentration is plotted against time.

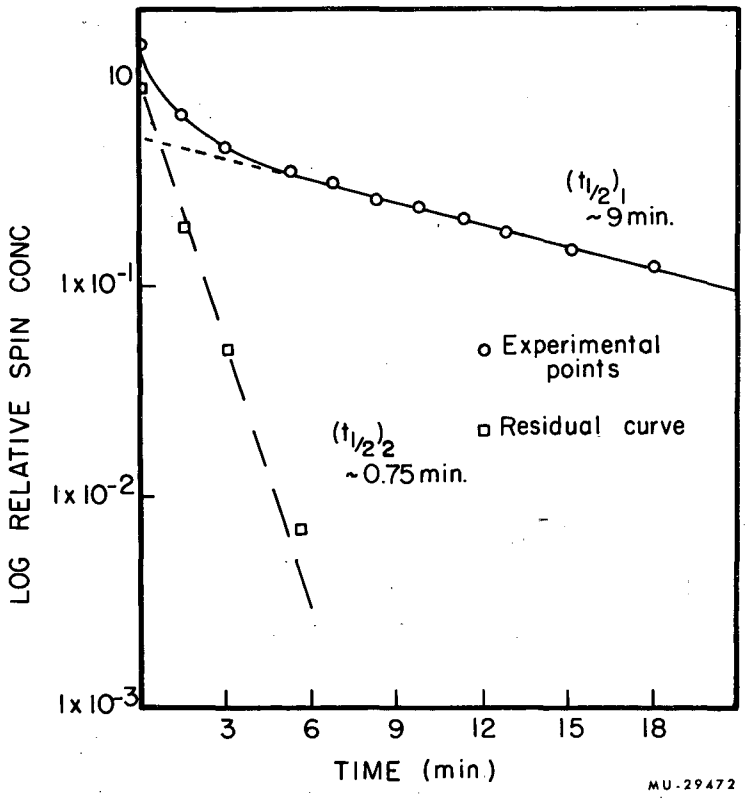

Fig. IV-4. Decay of photoinduced EPR signal in solution of 0.05 M p-chloranil in dioxane. The log of the relative spin concentration is plotted against time.

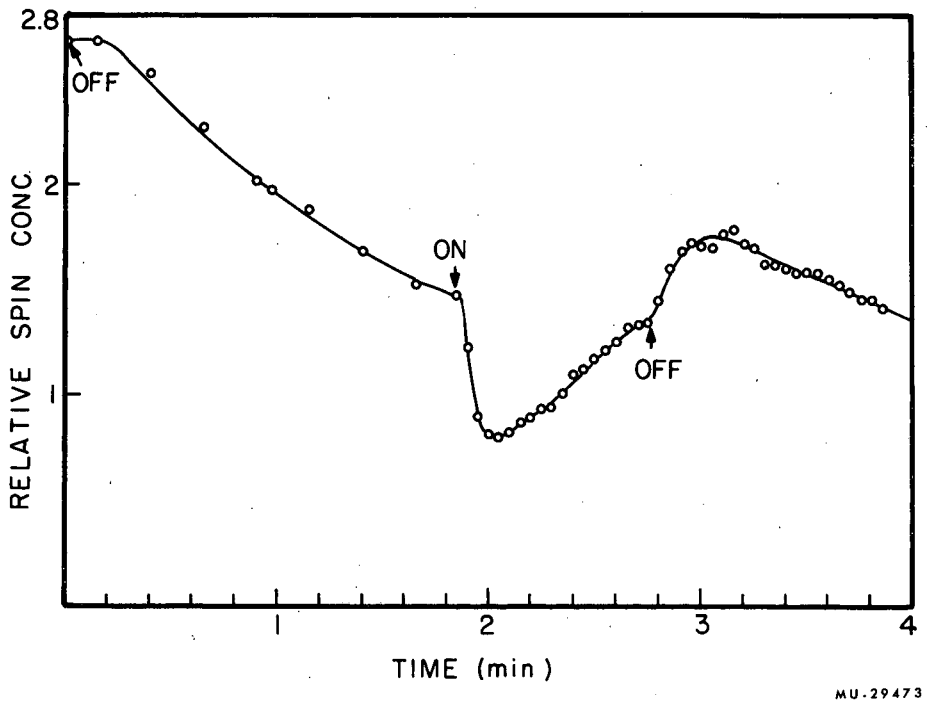

Fig. IV-5. Effects of irradiation on the EPR spin concentration of a solution of 0.05 M p-chloranil in dioxane. The relative spin concentration is plotted against the time of irradiation.

the recombination or the destruction of the species bearing unpaired electrons.

The final products in the above reactions have not been determined. Several possible reactions could have taken place. Chloranil, according to Schenck (39), can be photodimerized. Also, chloranil (40) frequently acts as a dehydrogenating agent, with the hydroquinone of chloranil as one of the final products. Since the purpose of the investigation was to study the nature of electronic transfer processes, attention was focused on the rapid initial rise of the signal, and the succeeding reactions were not analyzed further.

2. Conductivity

Irradiation of a solution of chloranil in dioxane resulted in a steady increase in the conductivity of the solution. No decrease was noted when the light was shut off. Both these facts seemed to indicate that a chemical reaction resulting in the formation of ionic species was taking place, and not the photoexcitation of an electron.

C. The Rise and the Decay of Fast EPR Signals

1. Introduction

The preliminary investigations of the preceding sections showed that certain charge-transfer systems exhibited EPR photosignals with rise and decay times of less than one second. In order to obtain more accurate values of the response times, the RC time constant of the EPR spectrometer was reduced to 30 msec. This, however, resulted in a reduction of the signal to noise ratio to 1, approximately. The difficulty was overcome by using an averaging technique (41). The sample was repeatedly irradiated with a pulse of light of 200 msec duration, and the photosignals resulting from these multiple irradiations were stored in a computer [Computer of

Average Transients (CAT), Mnemotron Corp., Pearl River, N. Y.]. The signal increased directly with the number of irradiations, whereas the noise increased only as the square root of the number of irradiations. At least 100 passes were made per sample, so that the signal to noise ratio was increased from 1 to 10. The duration of the light pulse was controlled with a camera shutter.

2. Results

The following systems were studied and showed photoinduced signals:

TABLE IV-II

Complex	Color	Signal Speed
p-chloranil-p-dioxane	Yellow	Fast
p-chloranil-THF	Yellow	Fast
o-chloranil-thiophene	Red	Fast
o-chloranil-CCl_4	Red	Slow
Solid o-chloranil	Red	Slow

All of the signals had g-values of very nearly 2. They were all approximately 15 gauss wide, showed no hyperfine structure, and were not symmetrical. Figures IV-6 through IV-8 show the experimental curves for the rise and the decay times of some of the systems. One of the principal difficulties in analyzing the date was determining when the shutter was opened. The 10-90% rise time for the shutter was approximately 10 msec. For the first three systems listed above, the maximum spin concentration was reached within 100 msec. After the shutter was closed,

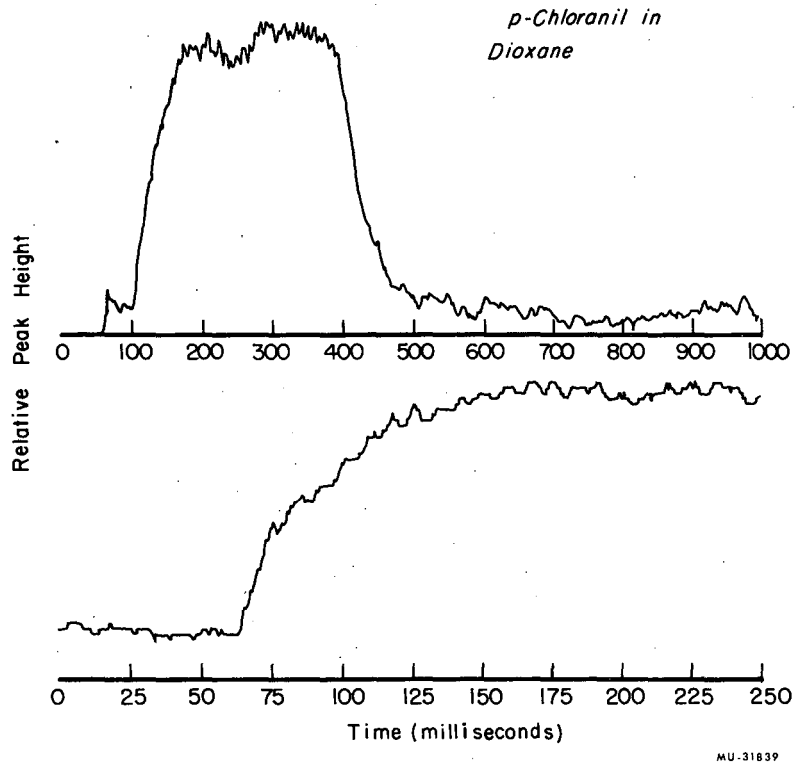

Fig. IV-6. a. Rise and decay of EPR signal for 0.05 M p-chloranil in dioxane (top). b. Rise time (expanded scale) (bottom).

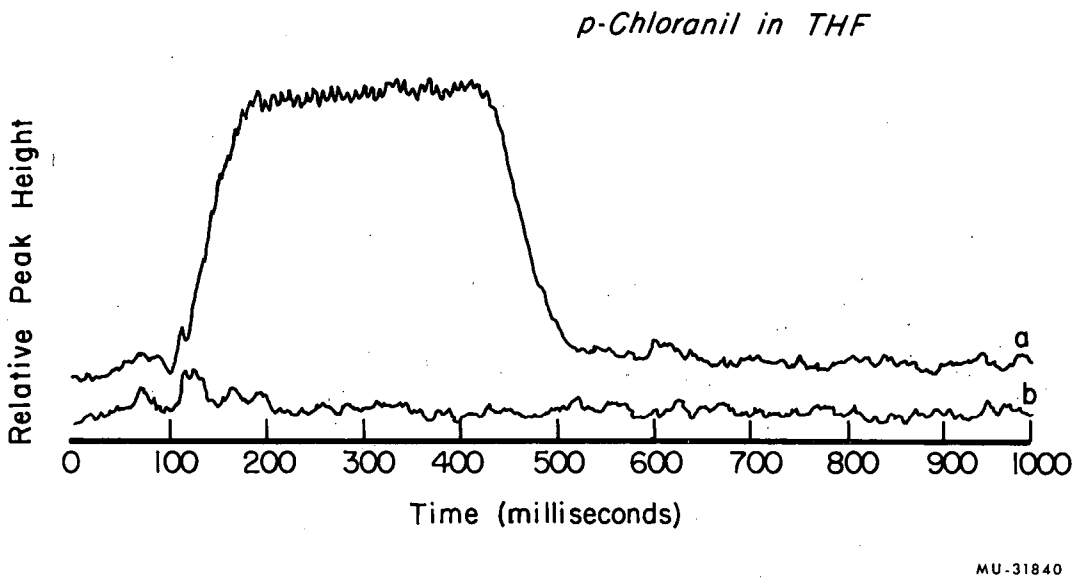

Fig. IV-7. a. Rise and decay of EPR signal for 0.05 M p-chloranil in tetrahydrofuran (THF). b. Signal off magnetic resonance to show noise.

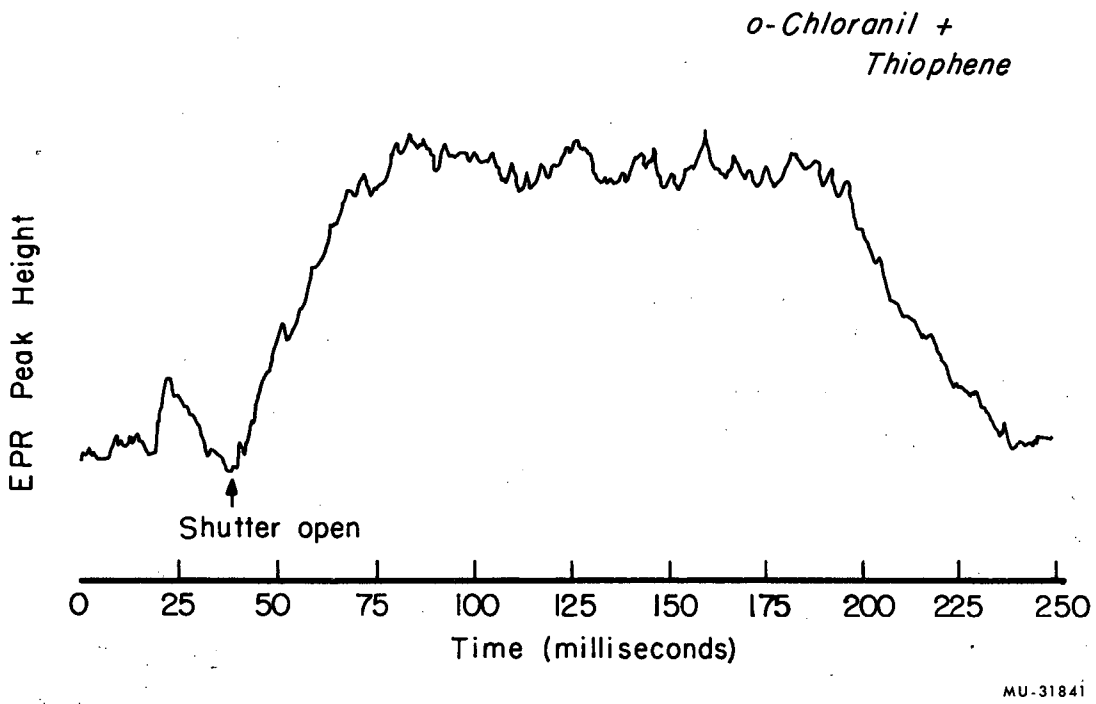

Fig. IV-8. Rise and decay of EPR signal for 0.05 M o-chloranil in thiophene. (Arbitrary units).

the spin concentration decayed to zero in 50 to 150 msec. The o-chloranil-thiophene system showed a photoinduced signal, while the p-chloranil-thiophene system did not. For controls, o-chloranil in CCl_4 and solid o-chloranil were also studied. In both cases a slowly growing EPR signal was observed, but no fast signal was seen. No signal was observed in any of the solvents alone. The photoinduced EPR signal seemed to result from an interaction between o-chloranil and thiophene. A signal did not appear if either the solvent or the solute alone were irradiated.

3. The Kinetics of the Rise and the Decay

An exponential growth can be represented analytically by

$$A = A_{ss} (1 - e^{-t/\tau}) \qquad \text{(IV.1)}$$

where

A = the amplitude of the EPR signal,

A_{ss} = the amplitude of the EPR signal at the steady state,

t = time,

τ = the time constant, the time required for A to rise to $(1 - 1/e)$ of its maximum value.

By rearranging Equation (IV.1) and taking logarithms,

$$\log (A - A_{ss}) = t/\tau + \log A \qquad \text{(IV.2)}$$

is obtained.

For exponential growth, a plot of $\log (A - A_{ss})$ vs. time should give a straight line. This is the case for p-chloranil-dioxane, as is shown in Figure IV-9. The rise is, therefore, exponential. In Figures IV-10 to IV-12 the decay curves for various samples are plotted. These data were obtained as before by adjusting the magnetic field to the point where the derivative of the absorption was at a maximum, then shutting

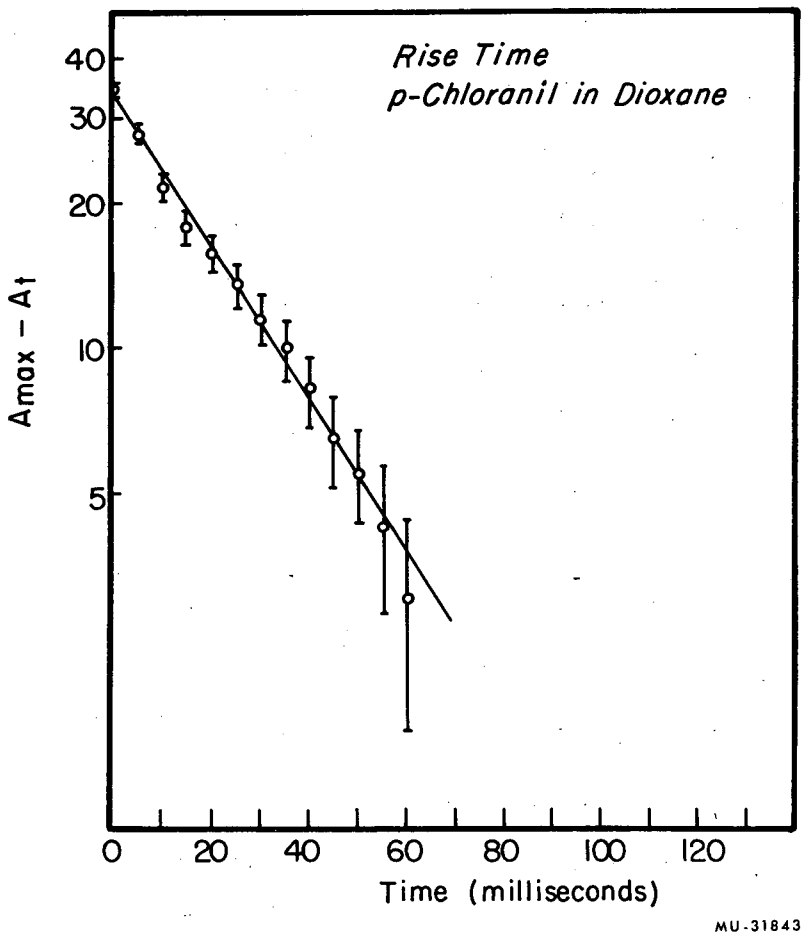

Fig. IV-9. Semilog plot of rise of EPR signal for 0.05 M p-chloranil in dioxane. A_{max} denotes maximum amplitude of signal in Fig. IV-6. Again the units are arbitrary. A_t denotes signal amplitude at time t, after light has been turned off.

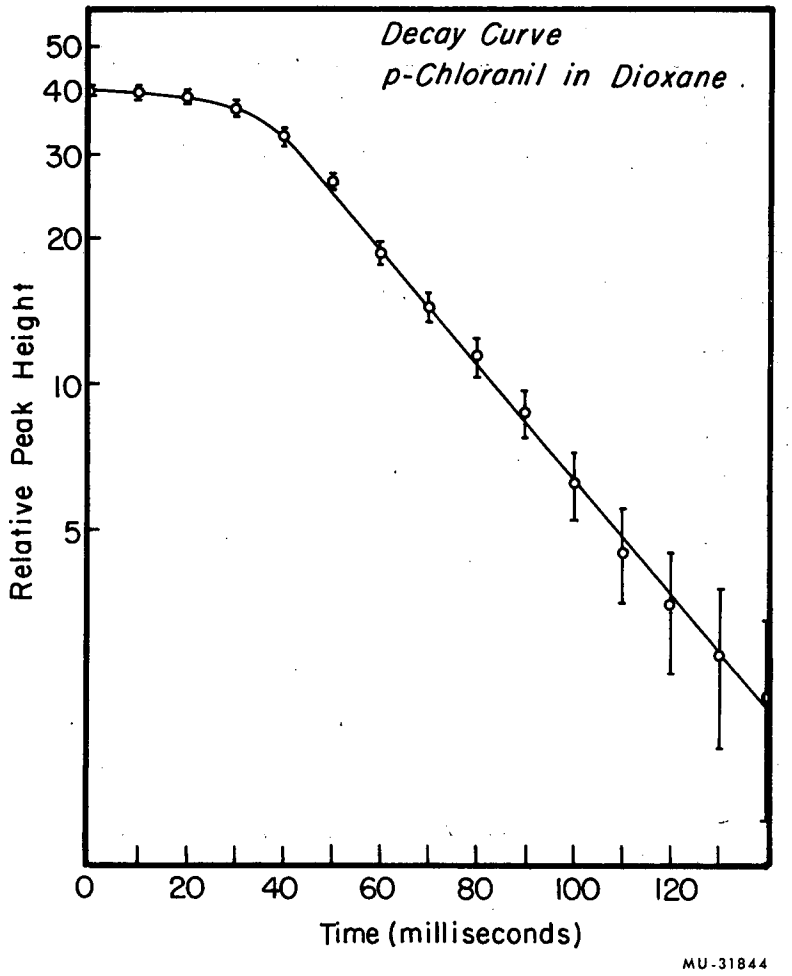

Fig. IV-10. Decay of EPR signal for 0.05 M p-chloranil in dioxane. The light was turned off at $t = 0$. Plot of log relative peak height vs time.

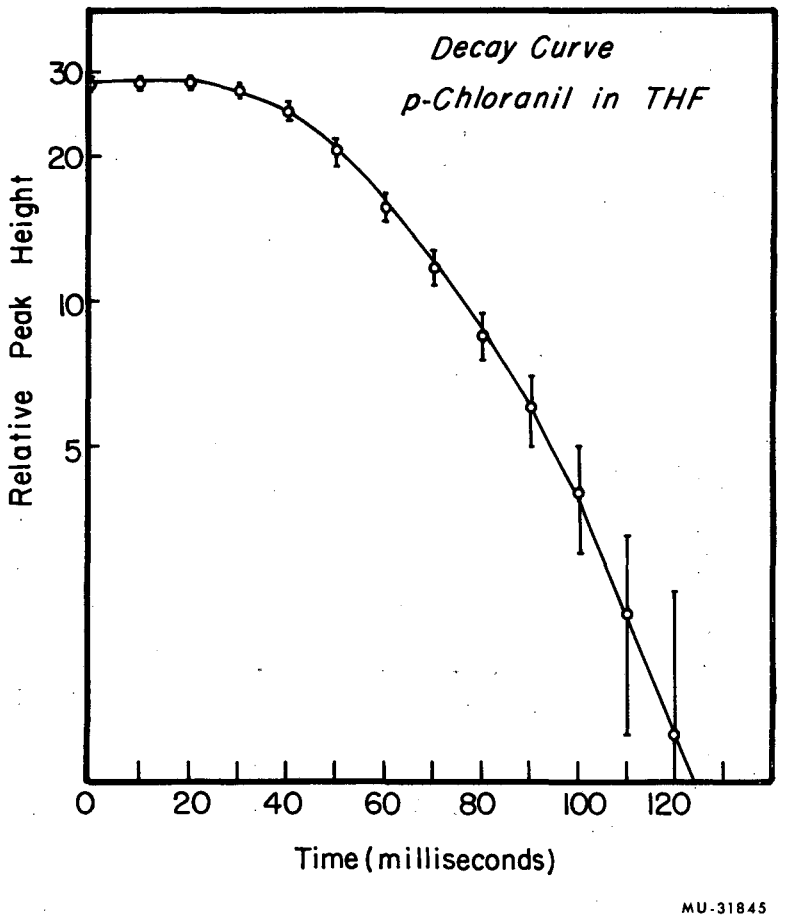

Fig. IV-11. Decay of EPR signal for 0.05 M p-chloranil in THF. The light was turned off at t = 0. Plot of log relative peak height vs time.

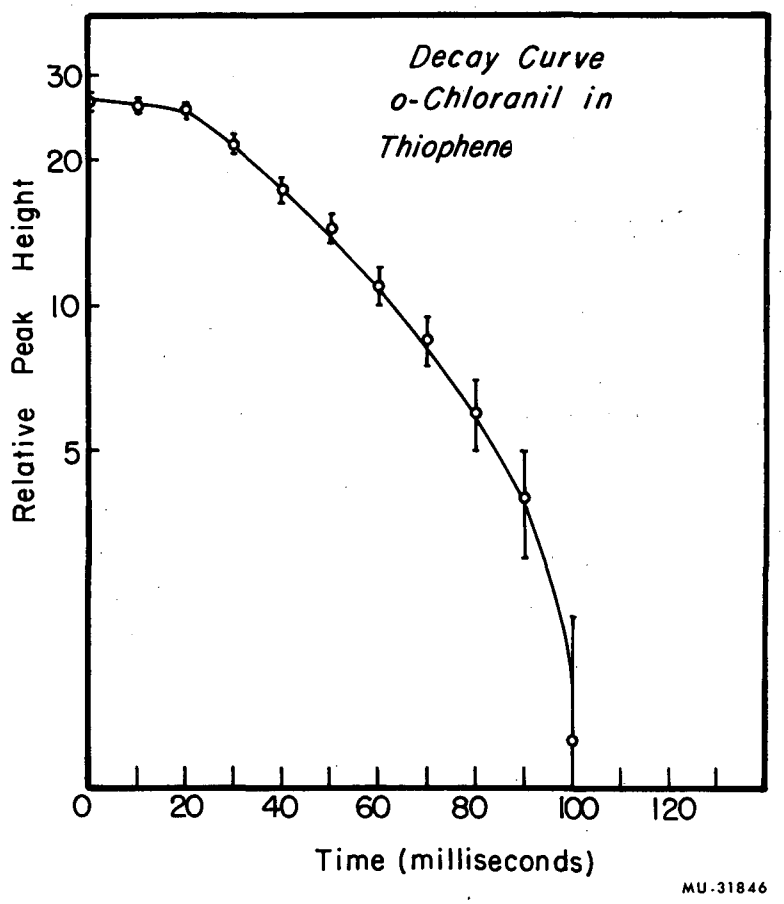

Fig. IV-12. Decay of EPR signal for 0.05 M o-chloranil in thiophene. The light was turned off at $\bar{t} = 0$. Plot of log relative peak height vs time.

off the light and observing the decrease in the maximum value. The decay curves are complicated, and may indicate the presence of several paramagnetic species.

In Figure IV-13 a comparison is drawn between the growth curves for p-chloranil and dioxane with and without a neutral density filter (Bausch and Lomb, O.D. 0.9) to reduce the intensity of irradiation to approximately 12.5% of its maximum value. The difference is small, although a longer rise time may be indicated for the case of the lower light intensity.

4. Temperature Effects

A preliminary investigation of the temperature dependence of the spin concentration showed that at 77° K there was no fast signal. However, a broad, long-lived signal was produced at 77° by irradiation. When the light was shut off, but the temperature kept at 77°, the signal amplitude remained the same. As the sample was warmed, the signal level gradually decreased until it vanished entirely at the melting point of the mixture.

5. Purification Procedures

p-Chloranil was recrystallized repeatedly from benzene after the hot solution had been treated with Norit. No impurities were detectable with thin-layer chromatography. p-Dioxane was prepared by vapor phase chromatography (VPC), using an Aerograph "Autoprep" (Wilkens Instrument and Research, Inc., Walnut Creek, Calif.) and a "Ucon polar" column. The purified dioxane showed no impurities in the VPC trace. Tetrahydrofuran (THF) was repeatedly distilled until only a trace of impurity could be found by VPC. Again a "Ucon polar" column was used.

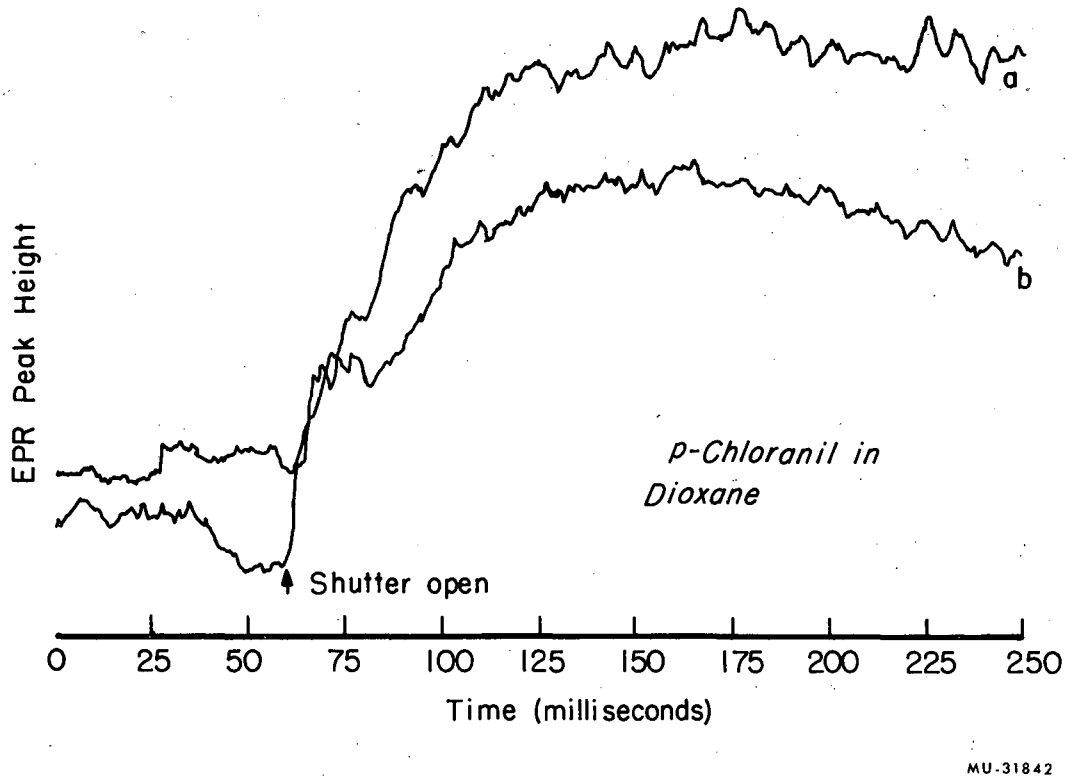

Fig. IV-13. a. Rise of EPR photosignal for 0.05 M p-chloranil in dioxane. b. Same, except light is attenuated to 12.5% of its intensity in (a) by means of a neutral density filter.

V. TETRAHYDROFURAN-TETRACYANOETHYLENE COMPLEX

A. The Complex

Tetracyanoethylene (TCNE) (42), a colorless cyanocarbon (Appendix I), was first prepared by Cairns, et al. in 1958. At that time Merrifield and Phillips (43) reported that TCNE readily dissolves in many organic solvents to produce intensely colored solutions. The colors were attributed, after Mulliken (9), to the formation of intermolecular charge-transfer complexes between the organic solvent donor molecules and the TCNE acceptor molecules. TCNE forms a charge-transfer complex with tetrahydrofuran (THF), as is indicated by the spectra in Figure V-1. Figure V-1a shows the spectrum of TCNE in ethylene dichloride, with maxima at 2650 Å and 2750 Å. The spectrum of TCNE in THF is shown in Figure V-1b. The two TCNE bands have been shifted to 2630 Å and 2710 Å, respectively, and a third band has appeared at 3000 Å. This latter band is characteristic of the charge-transfer complex. Vars (44) studied the TCNE-THF complex in chloroform solution and found the maximum to be at 3100 Å. This difference in maxima is not unexpected, as Mulliken's theory predicts an effect of the dielectric constant of the solution in the absorption maximum of the complex.

B. Photoinduced EPR in the TCNE-THF Complex

1. Introduction

TCNE negative ion radicals can be produced by irradiating a solution of TCNE-THF with a mercury lamp. This was first reported by Ward (45). The present work was designed to study the kinetics of the photoreaction and the effects of the intensity and the frequency of the light on the observed EPR signal. The measurements were made at room temperature, using a sample of 0.2 ml of a solution of 0.01 M TCNE in

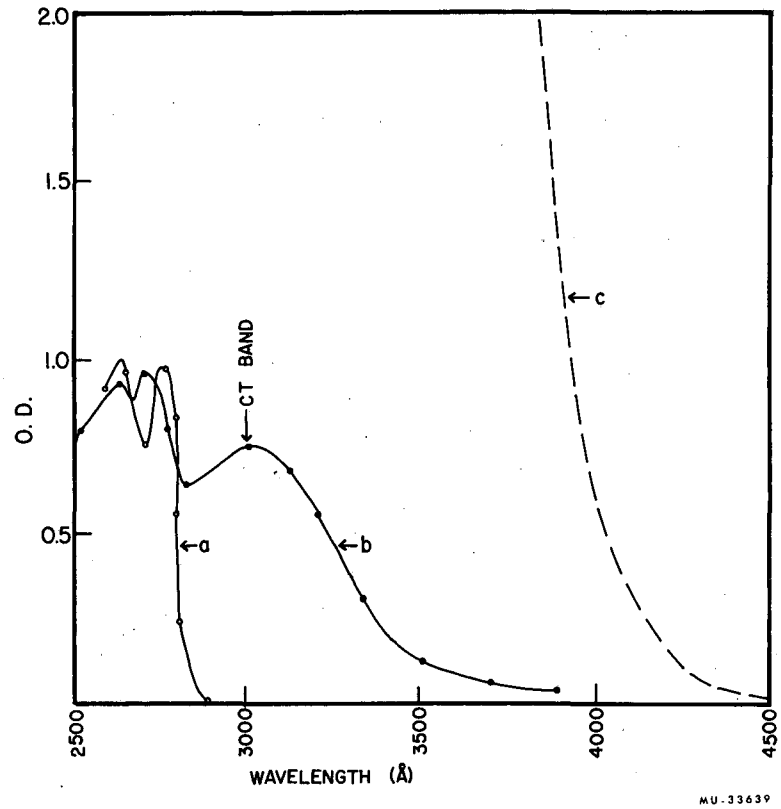

Fig. V-1. Optical absorption spectra demonstrating the formation of a charge-transfer complex between tetracyanoethylene and tetrahydrofuran. a. 2×10^{-5} M TCNE in CCl_4. b. 2×10^{-5} M TCNE in THF. c. 0.01 M TCNE in THF.

THF. The sample had been degassed and then sealed in a quartz tube. While initially there was no EPR signal in the dark, a resonance could be produced by light. The spectrum obtained is shown in Figure V-2. The 11-line hyperfine structure is characteristic of the TCNE negative ion radical (46). Nine of the lines, with intensity ratios of 1:4:10:16:19:16:10:4:1, result from the hyperfine splitting of the 4 ^{14}N atoms of the cyanide groups. ^{14}N has a nuclear moment of 1. The hyperfine splitting is given by 2I + 1, where I is the sum of the nuclear moments. The other two lines appear at the extremes of the spectrum and are caused by the ^{13}C splitting. The g-value of the central line is very nearly 2.0023, the value for a free electron. When the light was cut off with a shutter, the signal reverted almost to the zero level. A small residual signal persisted and remained constant throughout further irradiation. This level was taken as the base line.

2. Kinetic Data

Inserting cut-off filters between the light source and the sample showed that the absorption producing the EPR photosignal occurred in the TCNE-THF charge-transfer band, between 3000 Å and 4500 Å. Typical rise and decay curves are shown in Figure V-3. Kinetic analyses of the data are given in Figures V-4 through V-8. Figures V-7 and V-8 show the dependence of the steady-state level of the spin concentration on the square root of the light intensity. The decay curve indicates second order kinetics. The growth of the EPR photosignal as a function of time is shown in Figure V-6. After an initial rise as the square of the time, the signal grew as the hyperbolic tangent of the time.

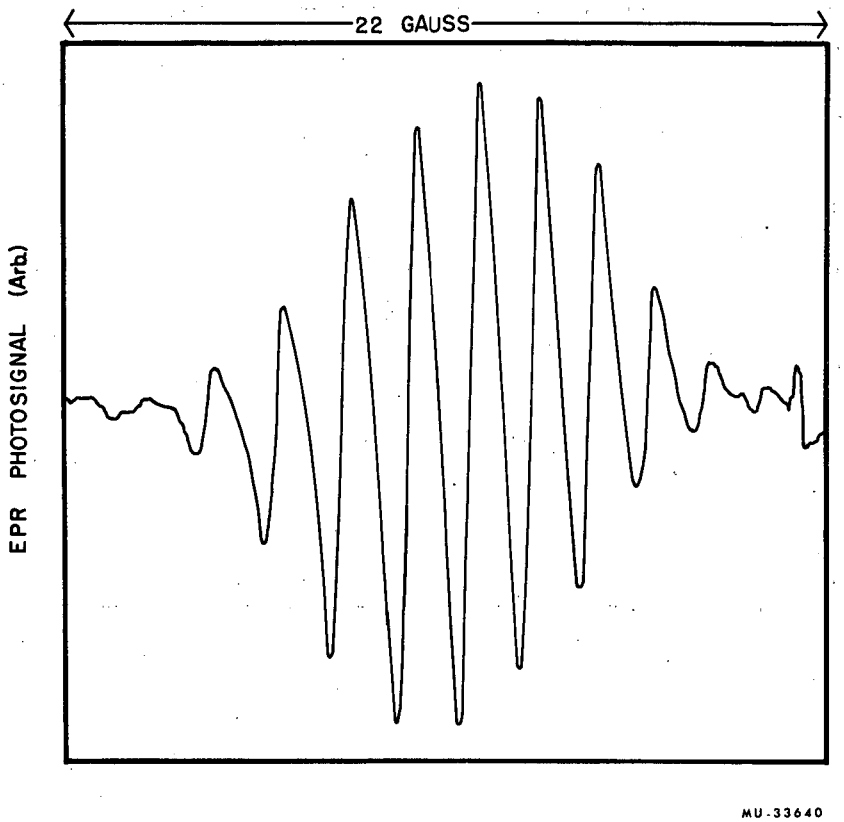

Fig. V-2. EPR spectrum of TCNE negative ion radical obtained by irradiating a solution of 0.01 M TCNE in THF. Nine of the 11 hyperfine lines result from the splitting of the 4 ^{14}N atoms of the cyanide groups. The additional 2 lines come from the ^{13}C splitting.

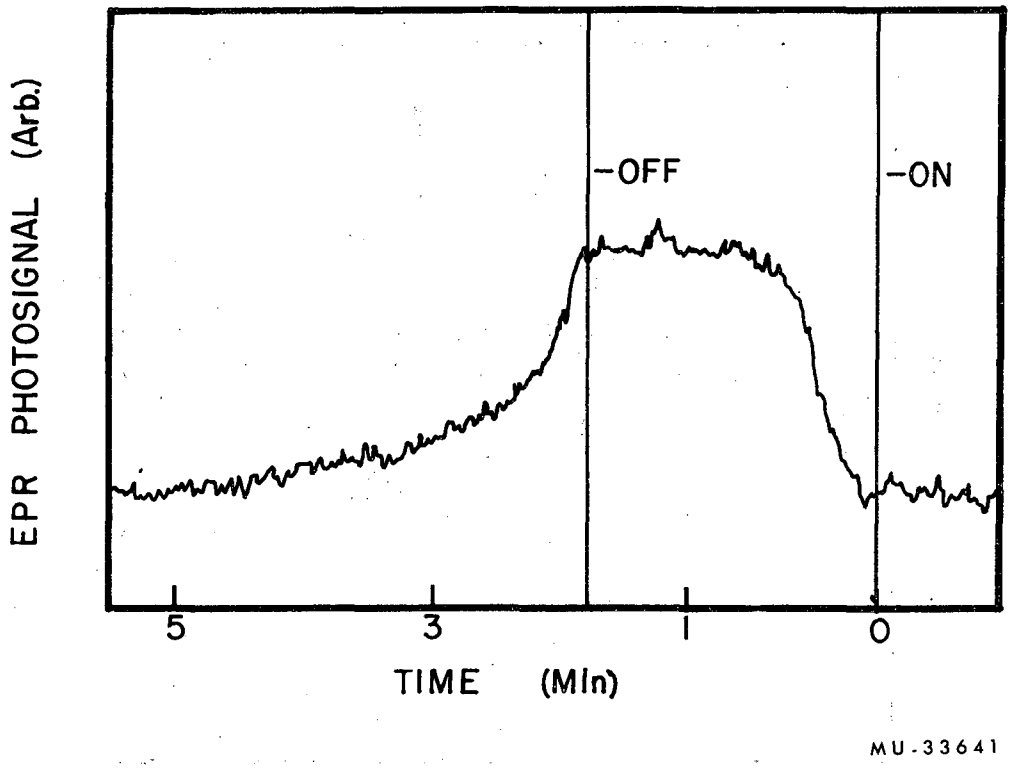

Fig. V-3. Rise and decay curves for the photoinduced EPR signal for 0.01 M TCNE in THF.

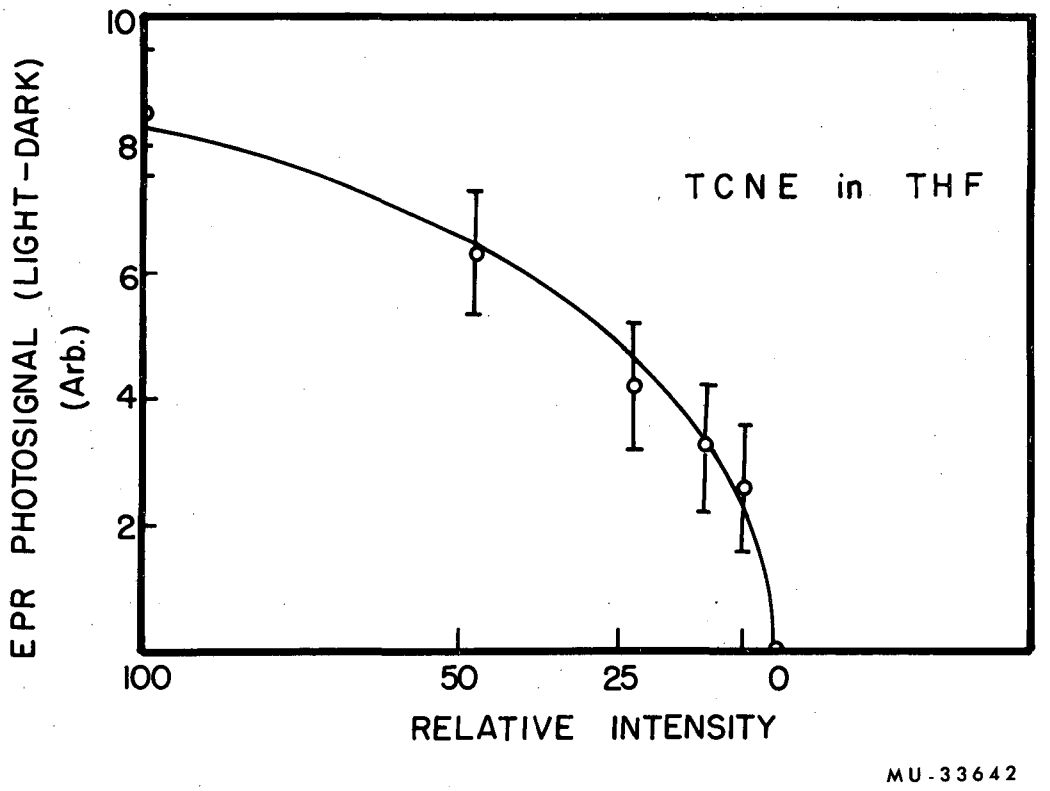

Fig. V-4. A linear plot of the steady-state value of the EPR photosignal for 0.01 M TCNE in THF vs the relative light intensity.

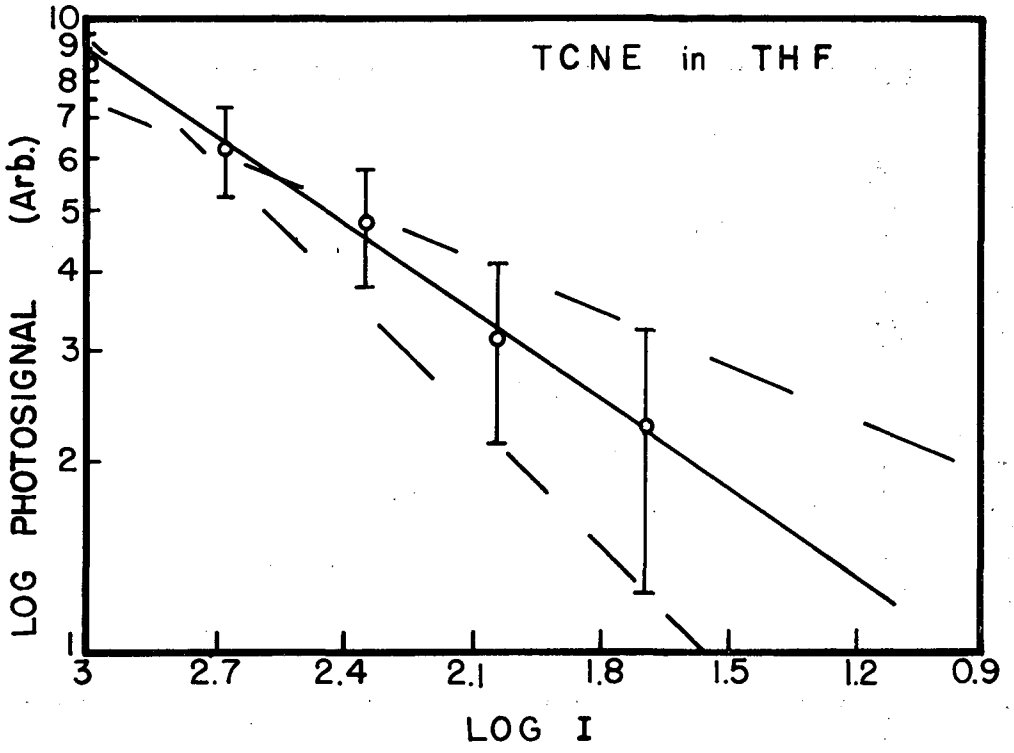

MU-33643

Fig. V-5. The steady-state value of EPR photosignal for a solution of 0.01 M TCNE in THF as a function of the light intensity. The log of the steady-state signal is plotted against the log of the light intensity.

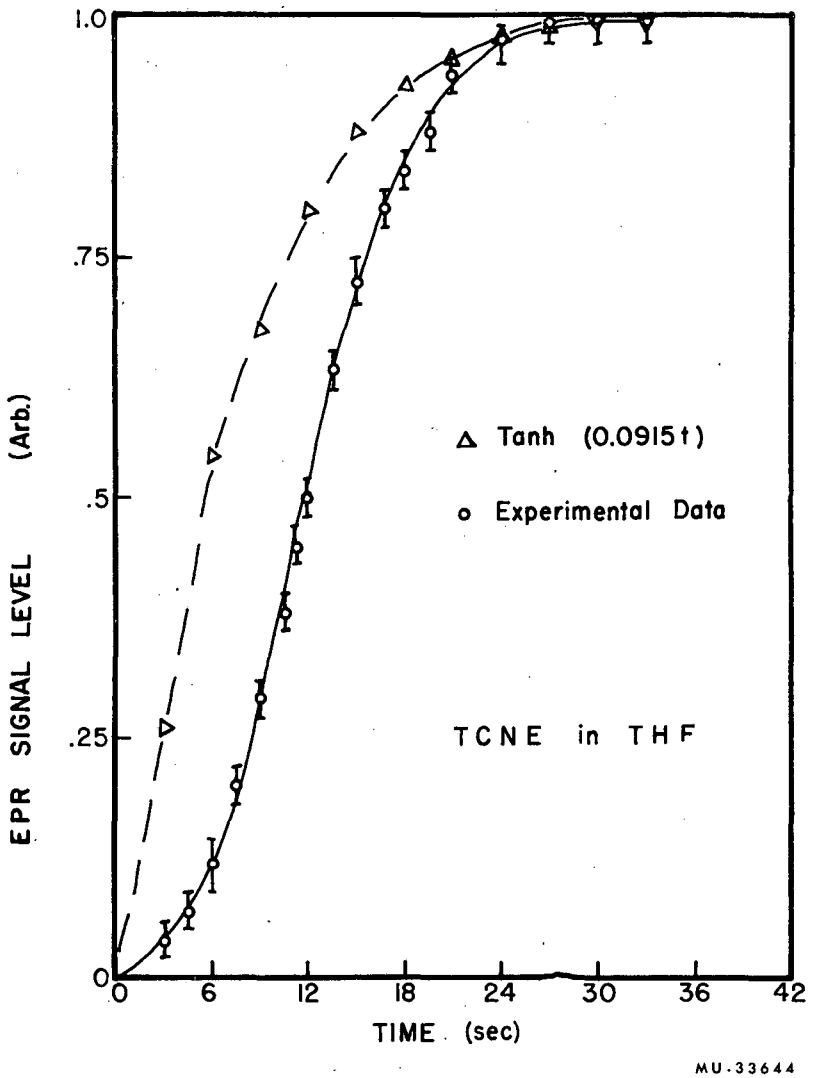

Fig. V-6. Growth curve for EPR photosignal for 0.01 M TCNE in THF. The hyperbolic tangent of 0.092t is plotted on the same axis.

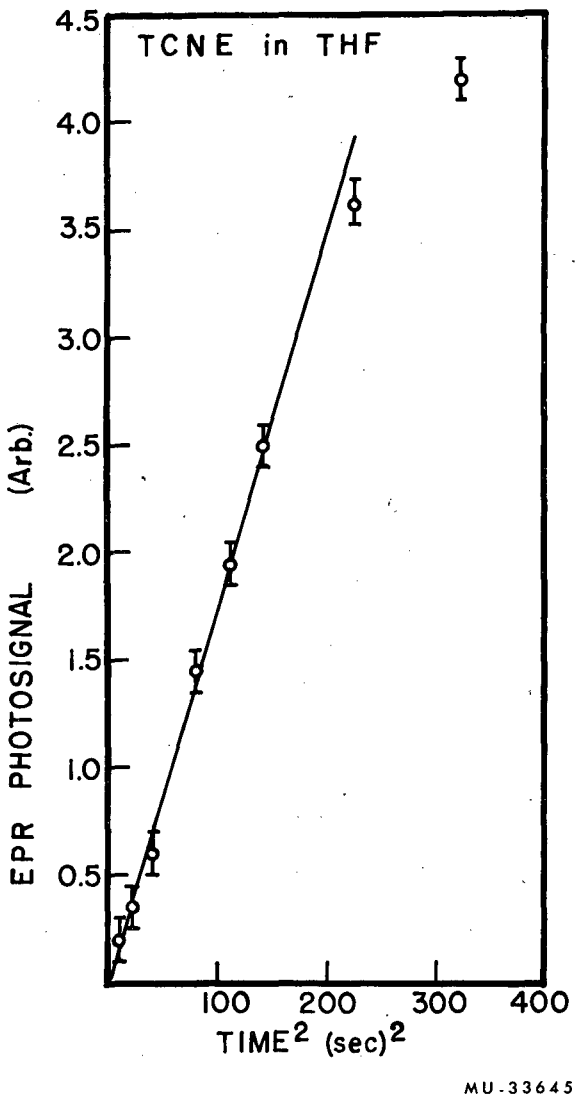

Fig. V-7. Growth of the EPR photosignal for 0.01 M TCNE in THF. The signal level is plotted against the square of the time.

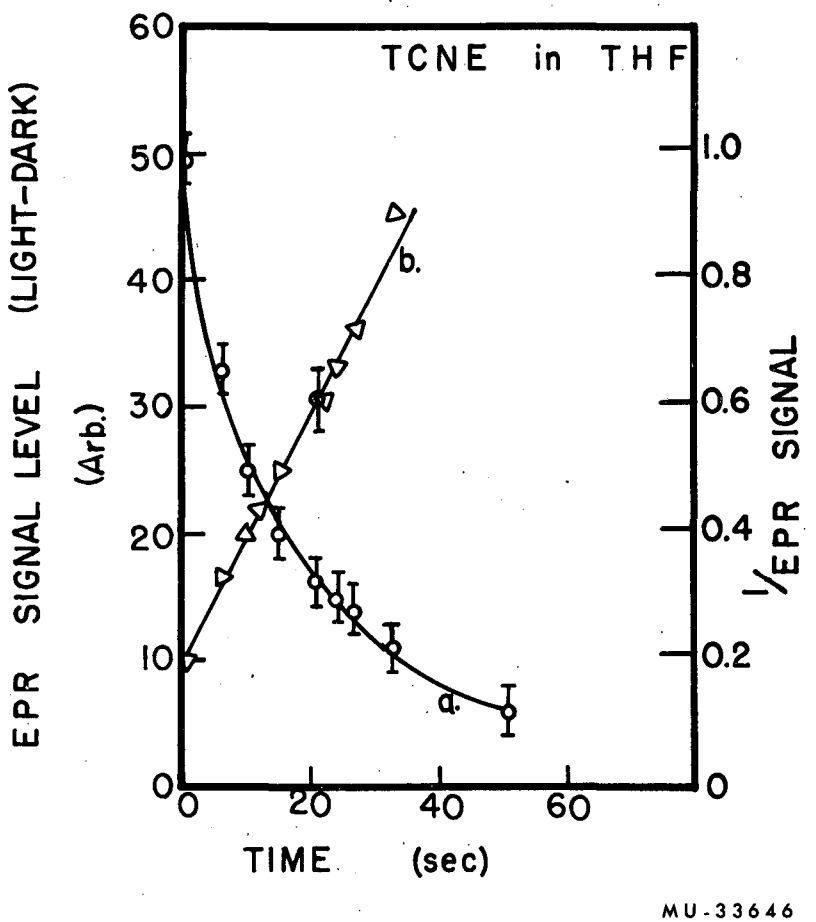

Fig. V-8. Decay of the EPR photosignal for 0.01 M TCNE in THF. a. Linear plot of EPR photosignal vs time. b. The reciprocal of the EPR photosignal vs time. The linear relation for (b) indicates that second order decay kinetics are followed.

3. Analysis of the Data

It was assumed initially that the reaction involved a simple and reversible transfer of an electron from the donor molecule to the acceptor molecule by the action of light. On this basis, the rate law

$$dn/dt = L - kn^2 \qquad (V.1)$$

was proposed,

where

L = the rate of the absorption of light energy by the solution, i.e., the intensity absorbed (quanta per second),

k = a rate constant for second order decay,

n = the concentration of the paramagnetic species.

It is assumed that the forward reaction is $C \rightarrow D^{\oplus} + A^{\ominus}$ and that its rate is directly proportional to the rate of the absorption of light by the solution. A further assumption is made that the decay of the spins occurs by a bimolecular recombination process, $D^{\oplus} + A^{\ominus} \rightarrow C$. Three phases of the reaction are described: First, the steady state, where the rate of formation of radicals by irradiation is exactly equal to the rate of the recombination of the $D^{\oplus}$ and $A^{\ominus}$ species; second, the decay when the light is shut off; and third, the growth of the signal.

a. The steady state. When the steady state has been reached,

$$(dn/dt)_{ss} = 0, \qquad (V.2)$$

and

$$n_{ss} = (L/k)^{1/2}. \qquad (V.3)$$

If, as is predicted by (V.3), the concentration of radicals in the steady state is proportional to the square root of the light intensity, a plot of log (n = spin concentration) vs. log (L = light intensity absorbed) should give a straight line with a slope of 0.5. The slope is, in fact,

0.47. Also, a plot of the spin concentration vs. the square root of the intensity gave a straight line. These results are indicated in Figures V-4 and V-5 and show that the steady-state spin concentration is dependent upon the square root of the light intensity.

b. Decay curve. When the light is shut off, L = 0 and the kinetic equation becomes

$$dn/dt = -kn^2. \qquad (V.4)$$

The integrated form of expression (V.4) is then

$$\int_{n_o}^{n} dn/n^2 = -\int_{t=o}^{t} kdt,$$

$$1/n - 1/n_o = kt$$

or

$$1/n = kt + 1/n_o.$$

It should also be noted that

$$1/\left(\frac{n_o}{2}\right) - 1/n_o = k\tau,$$

$$1/n_o = k\tau,$$

$$\tau = 1/kn_o,$$

where τ = the half-life of the radical, and

n_o = initial concentration of free radicals.

As is illustrated in Figure V-4, a plot of 1/n vs. t gives a straight line with intercept $1/n_o$ and slope of k. A value of 0.015 arbitrary units was obtained for k from the slope. It is also true for second order kinetics as indicated above, that $n_o = 1/k\tau$. For the same decay curve, n_o = 73 and k = 0.014 arbitrary units.

c. The growth curve. The integration of expression (V.1), as is illustrated below, gives

$$n = n_{ss} \tanh (Lk)^{1/2}\, t. \qquad (V.5)$$

The hyperbolic tangent is plotted on the same axis as the growth curve for the EPR in Figure V-6. The experimental data reach the hyperbolic tangent after an initial induction period, where the growth is as the square of the time.

d. Solution of the kinetic equation:

$dn/dt = L - kn^2$ (V.1)

Let

$$u = \sqrt{\frac{k}{L}}\, n$$

$$du = \sqrt{\frac{k}{L}}\, dn$$

$$dn = \sqrt{\frac{L}{k}}\, du$$

$$\frac{dn}{L-kn^2} = dt$$

$$\frac{\frac{dn}{L}}{1-(k/L)\,n^2} = dt$$

$$\frac{\sqrt{\frac{1}{Lk}}\, du}{1-u^2} = dt \quad \text{or} \quad \int_0^u \frac{du}{1-u^2} = \sqrt{Lk}\int_0^t dt$$

$$\tanh^{-1} u = (Lk)^{1/2}\, t$$

$$u = \tanh(Lk)^{1/2}\, t$$

$$n = \left(\frac{L}{k}\right)^{1/2} \tanh(Lk)^{1/2}\, t$$

$$n = n_{ss} \tanh (Lk)^{1/2}\, t \qquad (V.5)$$

e. Further analysis of the results. Although the rate equation (V.1) agrees with the steady state and with the decay state, it does not agree with the growth curve for the free radical concentration. The following reaction mechanism involving several intermediate steps is proposed:

$$D + A \rightarrow C, \qquad (V.6a)$$

(Because of the large excess of THF, it was assumed that essentially all of the TCNE molecules were complexed.)

$$C \rightarrow C^S, \qquad (V.6b)$$

(In this step the complex is excited to the excited singlet state by an incident photon. The reaction is directly proportional to the intensity of the light absorbed.)

$$C^S \rightarrow C, \qquad (V.6c)$$

(The excited singlet molecule relaxes to the ground state. This reaction proceeds according to a first order rate law, with rate constant k_2.)

$$C^S \rightarrow C^T, \qquad (V.6d)$$

(The excited singlet state goes to the excited triplet state. The first order rate constant is k_3.)

$$C^T \rightarrow C, \qquad (V.6e)$$

(The triplet excited state of the complex relaxes to the ground state. The rate constant is k_4.)

$$C^T \rightarrow D^{\oplus} + A^{\ominus}, \qquad (V.6f)$$

(The triplet state of the complex goes to the ionized components of the complex, $D^{\oplus}$ and $A^{\ominus}$. The rate constant is k_5.)

$$D^{\oplus} + A^{\ominus} \rightarrow C, \qquad (V.6g)$$

(The ions recombine to form the complex. The second order rate constant is k_6.).

If it is assumed that the life-time of the singlet state of the complex is so short that the concentration of the singlet species is always at the steady-state concentration, then from Equations b, c, and d the the expressions

$$dc^S/dt = L - (k_2 + k_3)\, c^S = 0 \qquad (V.7)$$

and

$$c^S = L/(k_2 + k_3) \tag{V.8}$$

can be obtained for the rate of change of the concentration and for the concentration of the singlet species, respectively. It is also necessary to assume that the concentration of the complex, C, is constant. This is reasonable because only a small fraction of the complex molecules are excited at any one time.

By similar arguments from Equations (V.6d), (V.6e), and (V.6f), expressions can be obtained for the rate of change of the concentration of the species in the triplet state,

$$dc^T/dt = k_3c^S - (k_4 + k_5)\,c^T, \tag{V.9a}$$

$$dc^T/dt = k_3L/(k_2 + k_3) - (k_4 + k_5)c^T. \tag{V.9b}$$

When expression (V.9b) is integrated,

$$\int_0^{c^T} \frac{dc^T}{[k_3L/(k_2 + k_3)] - (k_4 + k_5)c^T} = \int_0^t dt, \tag{V.10a}$$

$$= \left(\frac{1}{k_4 + k_5}\right) \ln \left| \frac{k_3L}{(k_2 + k_3)} - (k_4 + k_5)c^T \right|_0^{c^T} = t, \tag{V.10b}$$

$$\ln \left| \frac{k_3L}{(k_2 + k_3)} - (k_4 + k_5)c^T \right|_0^{c^T} = -(k_4 + k_5)t, \tag{V.10c}$$

$$\ln \left| \frac{k_3L}{(k_2 + k_3)} - (k_4 + k_5)c^T \right| - \ln \left| \frac{k_3L}{(k_2 + k_3)} \right| = -(k_4 + k_5)t, \tag{V.10d}$$

$$\frac{k_3L}{(k_2 + k_3)} - (k_4 + k_5)c^T = \frac{k_3L}{(k_2 + k_3)}\, e^{-(k_4 + k_5)t}, \tag{V.10e}$$

an expression is obtained for c^T, the concentration of the species in the triplet state

$$c^T = \frac{k_3L}{(k_2 + k_3)(k_4 + k_5)} \left[1 - e^{-(k_4 + k_5)t}\right]. \tag{V.10f}$$

An expression for n, the concentration of the negative ion radical species (in this case, $TCNE^-$) may be obtained from (V.6f) and (V.6g),

$$dn/dt = k_5\, c^T - k_6 n^2. \qquad \text{(V.11)}$$

In attempting to obtain a solution of Equation (V.11), it is helpful to consider three cases:

Case (1). The light intensity goes to zero. Then c^T goes to zero, and (V.11) becomes

$$dn/dt = -\, k_6\, n^2, \qquad \text{(V.11a)}$$

which is precisely the equation for second order decay which was obtained earlier as Equation (V.4).

Case (2). The steady state. At the steady state, $t = t_{ss}$ and

$$c^T = \left[k_3 L/(k_2 + k_3)\,(k_4 + k_5)\right]\left[1 - e^{-(k_4 + k_5)t_{ss}}\right]. \qquad \text{(V.11b)}$$

Since t_{ss} is large, (V.11b) becomes

$$c^T = k_3 L/(k_2 + k_3)\,(k_4 + k_5). \qquad \text{(V.11c)}$$

However, it can be seen from Equation (V.11) that at the steady state

$$n_{ss} = (k_5/k_6)\, c^T \qquad \text{(V.11d)}$$

or

$$n_{ss} = L^{1/2}\, [k_3\, k_5/(k_2 + k_3)\,(k_4 + k_5)]^{1/2}. \qquad \text{(V.11e)}$$

As before, there is a dependence of the steady-state concentration of spins upon the square root of the light intensity.

Case (3). The rise time. The rate of increase of the concentration of n is given by

$$dn/dt = \frac{L\, k_3\, k_5}{(k_2 + k_3)\,(k_4 + k_5)} \quad 1 - e^{-(k_4 + k_5)\, t} - k_6\, n^2. \qquad (V.12)$$

By letting $\alpha = \dfrac{k_3\, k_5}{(k_2 + k_3)\,(k_4 + k_5)}$ and $\beta = (k_4 + k_5)$,

expression (V.12) becomes

$$dn/dt = \alpha\, L\, (1 - e^{-\beta t}) - k_6\, n^2$$

or

$$dn/dt + k_6\, n^2 - \alpha\, L\, (1 - e^{-\beta t}) = 0. \qquad (V.13)$$

Equation (V.13) is a first order non-linear differential equation and cannot in general be solved. It is a form of Riccati's Equation (47). Certain Riccati Equations can be transformed into second order linear equations, which can be solved. However, Equation (V.13) is not susceptible to this approach. Two other approaches will be tried: making simplifying assumptions and making iterated approximations (e.g., Picard's Method).

Simplifying assumptions. Initially when the light is turned on, $n = 0$, so that (V.13) becomes

$$dn/dt - \alpha\, L\, (1 - e^{-\beta t}) = 0. \qquad (V.14)$$

By integrating (V.14)

$$\int_0^n dn = \int_0^t \alpha\, L(1 - e^{-\beta t})\, dt,$$

an expression for n,

$$n = \left[\alpha\, Lt + \frac{e^{-\beta t}}{\beta}\right]_0^t = \frac{\alpha\beta Lt + e^{-\beta t}}{\beta} - 1/\beta$$

or

$$n = \frac{\alpha\beta t + e^{-\beta t} - 1}{\beta} \qquad (V.15)$$

is obtained. For small t, the approximation

$$e^{-\beta t} = 1 - \beta t + \beta^2 t^2 \text{ may be made.}$$

When this is substituted into (V.15), the expression

$$n = \alpha\beta L t + 1 - \beta t + \beta^2 t^2 - 1 \text{ or } n = \beta t^2 + t(\alpha L - 1)$$

is obtained, which predicts a parabolic rise of the signal with time. If in Equation (V.16) we assume that $\alpha L - 1 \sim 0$, then (V.16) becomes

$$n = \beta t^2. \qquad (V.16a)$$

For very large t (V.13) becomes

$$dn/dt = \alpha L - k_6 n^2, \qquad (V.17)$$

which gives the hyperbolic tangent rise (see p. 64),

$$n = n_{ss} \tanh (k_6/\alpha)^{1/2} L^{1/2} t. \qquad (V.18)$$

<u>Picard's Method.</u> Successive integrations of the form

$$y_{n+1}(t) = \int_0^t [(y_n(t))^2 + \alpha L(1 - e^{-\beta t})]\, dt$$

indicate that the solution of (V.13) shows an initial rise as approximately the square of time, which is then followed by a cutoff.

4. <u>Summary</u>

The rate equation

$$dn/dt + k_6 n^2 - \alpha L (1 - e^{-\beta t}) = 0 \qquad (V.13)$$

predicts that the EPR signal should grow initially as the square of the time and then, as the steady state is approached, as the hyperbolic tangent of the time. Both of these effects were observed experimentally. Likewise, the theory agrees with the observed dependence of the steady-state spin concentration on the square root of the light intensity and with the second order decay kinetics. In the next section, correlations

will be drawn between the photoinduced EPR signals and the photoconductivity results.

Although tetracyanoethylene negative ion radical was identified by EPR, no evidence was found for a corresponding positive ion radical. It has often been the case with EPR studies of organic solutions that a negative ion radical could be detected, but no positive ion radical observed. Few explanations have been offered for this phenomenon. In the case of TCNE-THF the most likely positive ion radical is $THF^{\oplus}$. The kinetic scheme presented above assumed that $THF^{\oplus}$ is formed and that it remains in solution until recombination with $TCNE^{\ominus}$ occurs. It seems highly unlikely that the THF positive ion radicals could combine with one another; the coulombic repulsion would be too great. A possible mechanism to prevent the observation of $THF^{\oplus}$ ion is uncertainty or exchange broadening. If the hole on a $THF^{\oplus}$ ion were free to migrate rapidly from one THF molecule to another, delocalization of the electron would result, and the $THF^{\oplus}$ signal could be broadened below the level of detectability. The argument is illustrated in Table V-I. Such a mechanism might be expected to lead to electronic conductivity in the solution.

TABLE V-I

Kinetic Scheme Showing Formation of $TCNE^{-}$ Ions

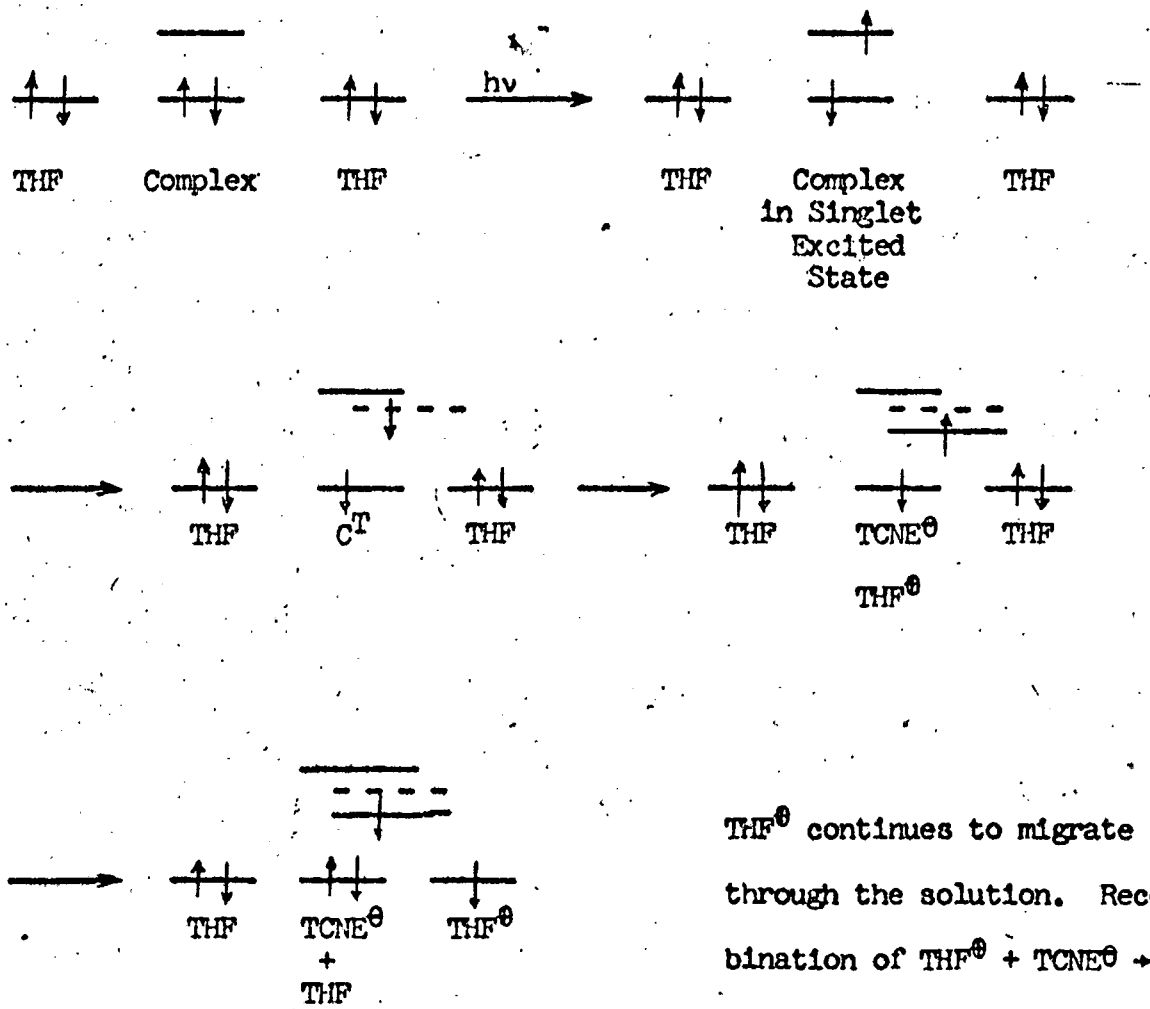

$THF^{\oplus}$ continues to migrate through the solution. Recombination of $THF^{\oplus}$ + $TCNE^{\ominus}$ → C → THF + TCNE occurs when $THF^{\oplus}$ has migrated to a $TCNE^{\ominus}$ site.

5. Experimental (48,49,50,51).

a. The electron paramagnetic resonance spectrometer. The EPR data were obtained using a microwave spectrometer consisting of a 9 gigacycle/sec klystron, a reflection cavity, and a crystal detection unit. The spectrometer magnet, which had been constructed in this laboratory, had pole pieces 6 inches in diameter and was powered with a Varian V2200 magent power supply. A Varian V4560, 100 kilocycle/sec, phase-sensitive field modulation unit was used for crystal detection. A 60 kilocycle/sec automatic frequency control (AFC) unit that had been constructed in this laboratory was also used. The measurements were made in a Varian V4531 rectangular cavity (TE_{103} model) with slots for irradiation. The spectrometer was calibrated by comparing the observed signal with a standard of 5×10^{14} spins of Cr^{+++} in an MgO host. The g-value for the standard was 2.0023.

b. The light sources and the optics. The light source was a Westinghouse H33-1-CD 400 watt mercury vapor lamp, focused onto the slots of the cavity by two glass lenses. The glass case of the lamp cut off all wavelengths shorter than 3100 Å. The total rated output (52) from 3100 Å to 3500 Å was 0.54 watts. This corresponds to 1.6×10^{16} quanta per second, assuming 3300 Å quanta. Over the region, 3500 Å to 4500 Å, the output was 30.2 watts, or, assuming 4000 Å quanta, 6×10^{19} quanta/sec. Cut-off filters were used to determine which wavelengths were producing the effect. The intensity of irradiation was varied by inserting a series of neutral density filters between the light source and the sample. These were of nominal transmission values of 5%, 25%, and 50%. The filters were calibrated using a Cary 14R recording spectrophotometer and were found to have transmission values of 4.7%, 22%, and 47.5%.

It is estimated that 1% of the rated intensity of the lamp reached the sample.

c. Materials. Eastman Kodak tetrahydrofuran was initially dried with potassium hydroxide tablets and then treated with lithium aluminum hydride. The sample was refluxed for two hours and then distilled. The first 100 ml portion of the distillate was discarded. The portion collected boiled at 65.5°. Eastman Kodak White Label tetracyanoethylene was used without further purification. All measurements were made on freshly prepared samples. After several days a faint pinkish tinge appeared in the TCNE-THF solution. Samples were prepared by the following procedure: 0.2 ml of a solution of 0.01 M TCNE in THF were placed into a quartz tube having an outside diameter of 4 mm. The sample was degassed by 5 freeze-pump-thaw cycles. The minimum pressure read was 7×10^{-6} Torr at 77° K, at which point the sample tube was sealed.

C. Photoconductivity in TCNE-THF Solution

1. Introduction

The detection of a rapid photoinduced EPR signal in TCNE-THF solution charge-transfer complex suggested that photoconductivity might be observed as well. Using the apparatus described in Section V.C.5, photoconductivity has been seen in a solution of 0.01 M TCNE in THF. Once the initial observation had been made, the signal was studied as a function of the wavelength and the intensity of the incident light. As in the case of the photoinduced EPR, cut-off filters were used to show that the absorption causing the photoconductivity took place in the tail of the charge-transfer band of the complex. Figure V-9 shows the photosignal growth curve. The signal level as a function of light intensity is plotted in Figure V-10. Kinetic studies are shown in Figures V-11 through V-14. Figure V-15 shows the photosignal as a function of the applied voltage. All measurements were made with the applied potential less than 0.4 volts. In this region the current vs. voltage characteristic was very nearly linear. A general review of photoconductivity in solids has been given by Bube (53). Meier (54) has reviewed some of the work on solution photoconductivity.

2. Analysis of the Results

The specific resistance or resistivity of a liquid is the resistance in ohms of a column of the liquid one cm long and one cm^2 in cross section. The conductivity is the reciprocal of the resistivity and may be expressed as

$$\sigma = ne\mu_n + pe\mu_p, \qquad (V.19)$$

where

p = the concentration of the positive charge carriers,

n = the concentration of the negative charge carriers,

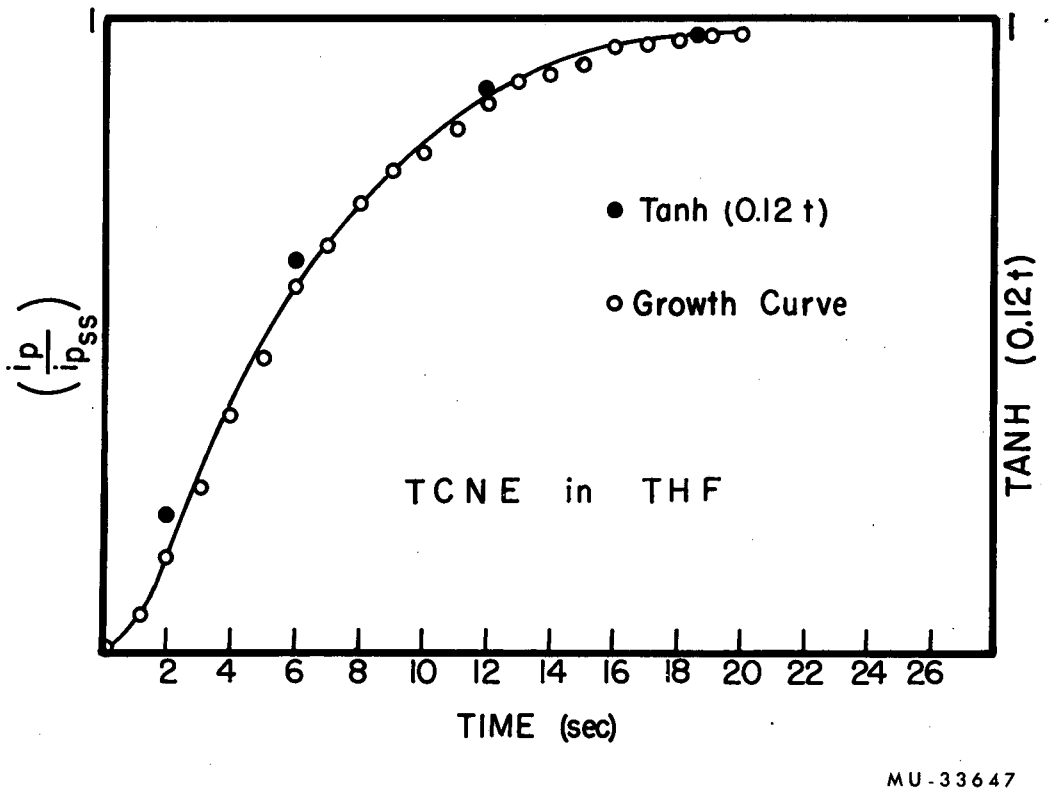

Fig. V-9. Growth curve for the photoconductivity of 0.01 M TCNE in THF. (Signal level)/(Steady-state signal level) is plotted against time. The black dots indicate the hyperbolic tangent of 0.12 t. The applied potential was 0.09 volts.

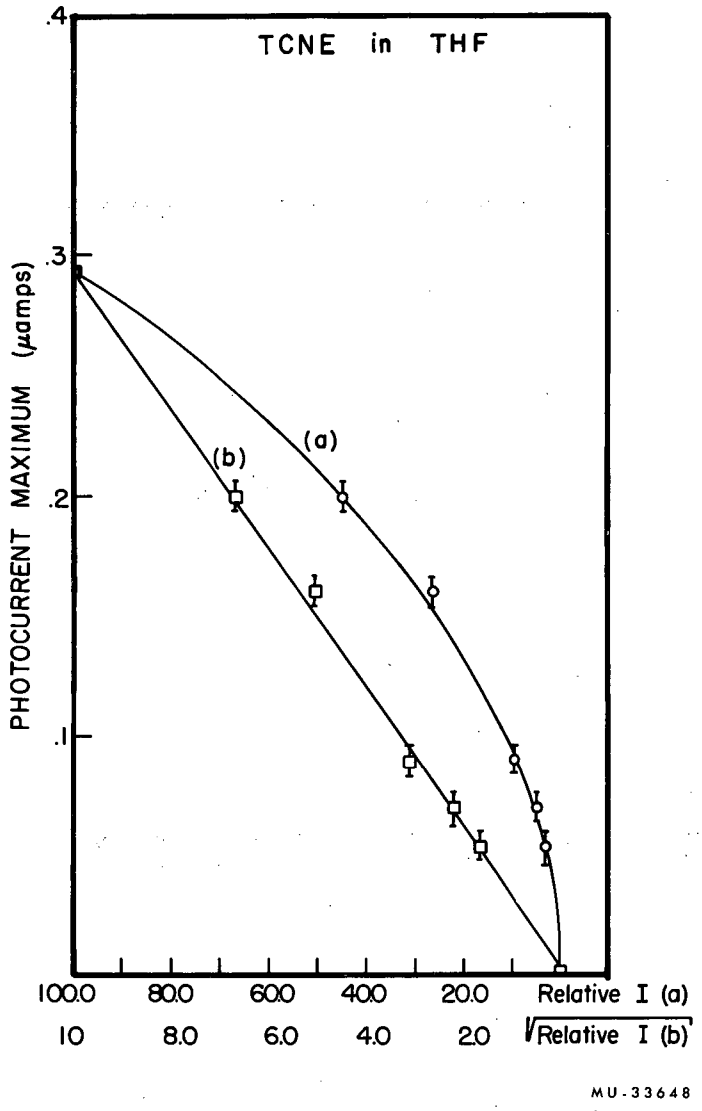

Fig. V-10. Steady-state photocurrent vs light intensity for 0.01 M TCNE in THF. a. Steady-state photocurrent vs relative light intensity. b. Steady-state photocurrent vs the square root of the relative light intensity. The applied potential was 0.09 volts.

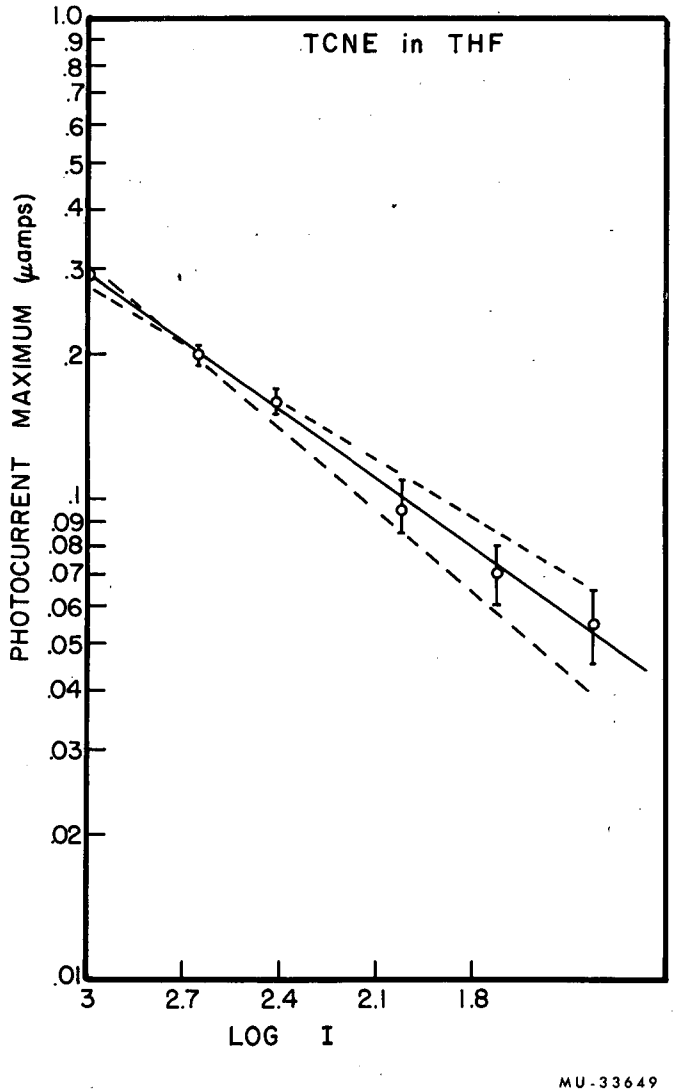

Fig. V-11. Steady-state photocurrent for 0.01 M TCNE in THF vs the log of the relative light intensity. The applied potential was 0.09 volts.

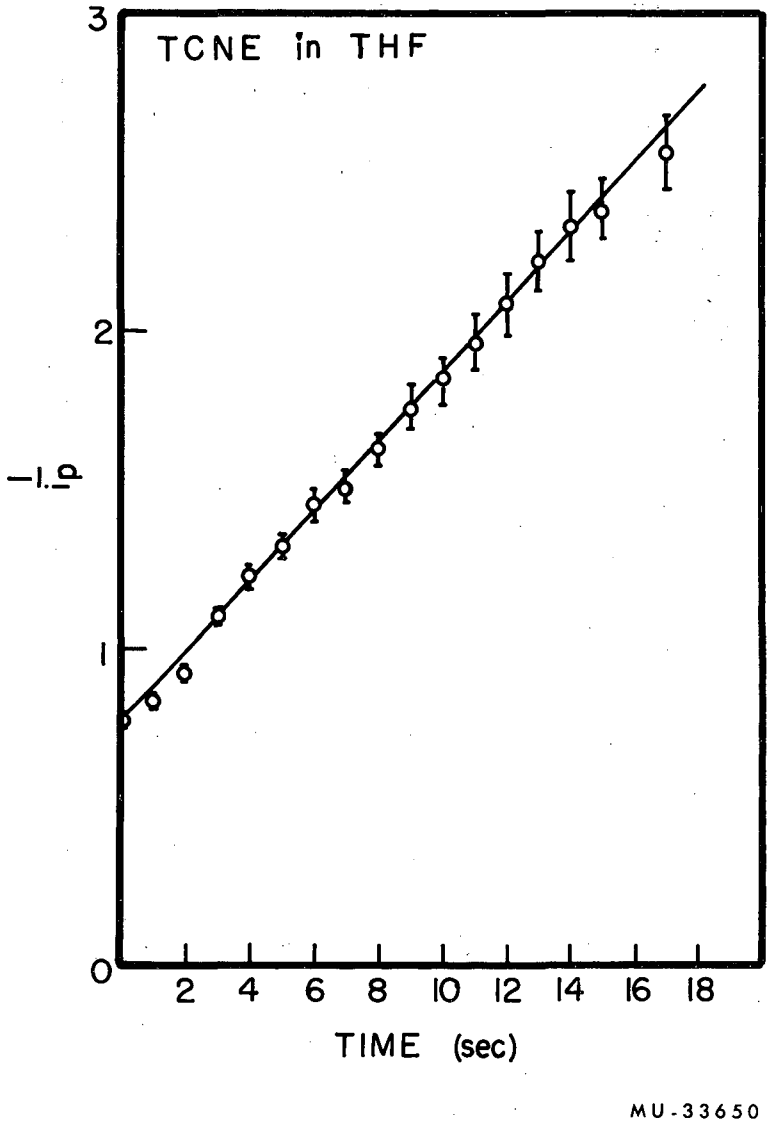

Fig. V-12. Decay of the photocurrent for 0.01 M TCNE in THF. The reciprocal of the photocurrent is plotted against the time of decay; 0.09 volts is the applied potential.

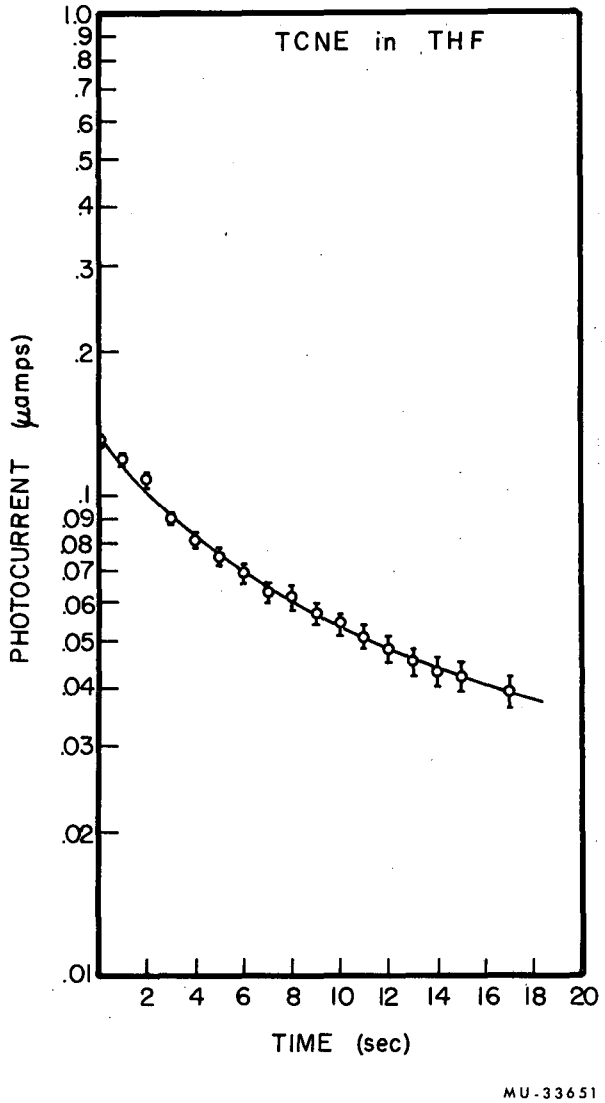

Fig. V-13. Decay of the photocurrent for 0.01 M TCNE in THF. The log of the photocurrent is plotted against the time of decay. First order decay is not followed.

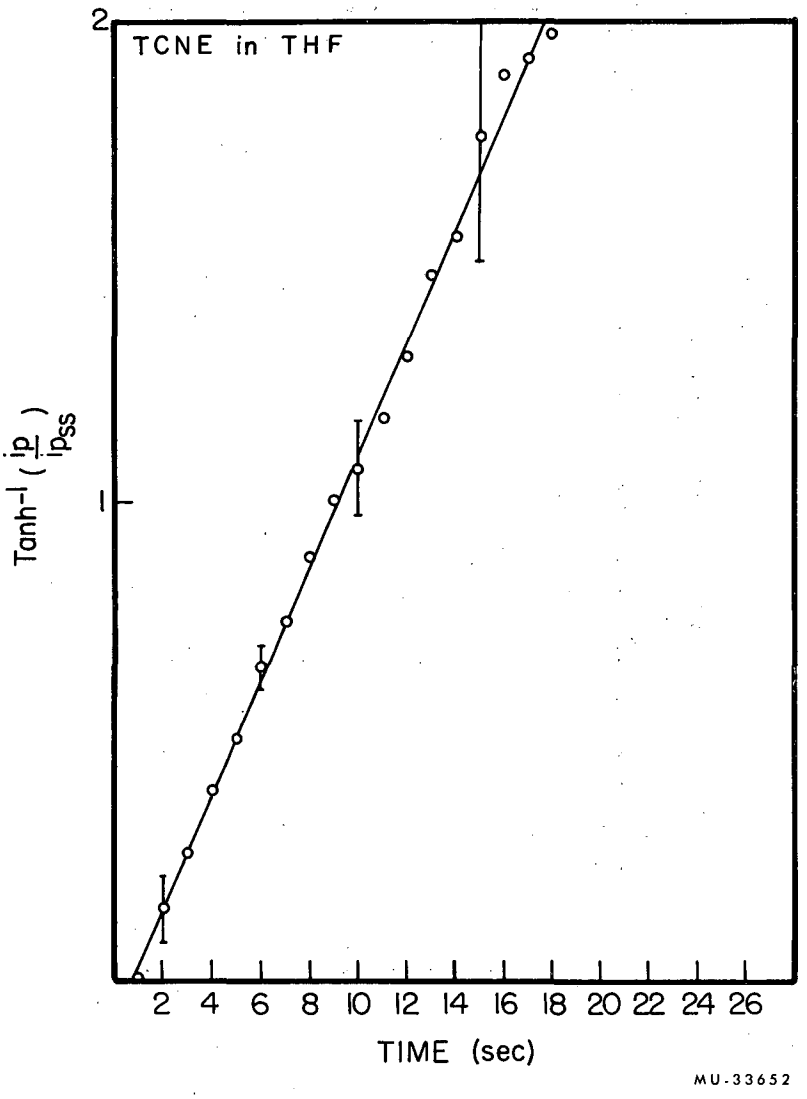

Fig. V-14. The growth of the photocurrent for 0.01 M TCNE in THF. The inverse hyperbolic tangent of (photocurrent/ steady-state photocurrent) is plotted against time. The applied potential was 0.09 volts.

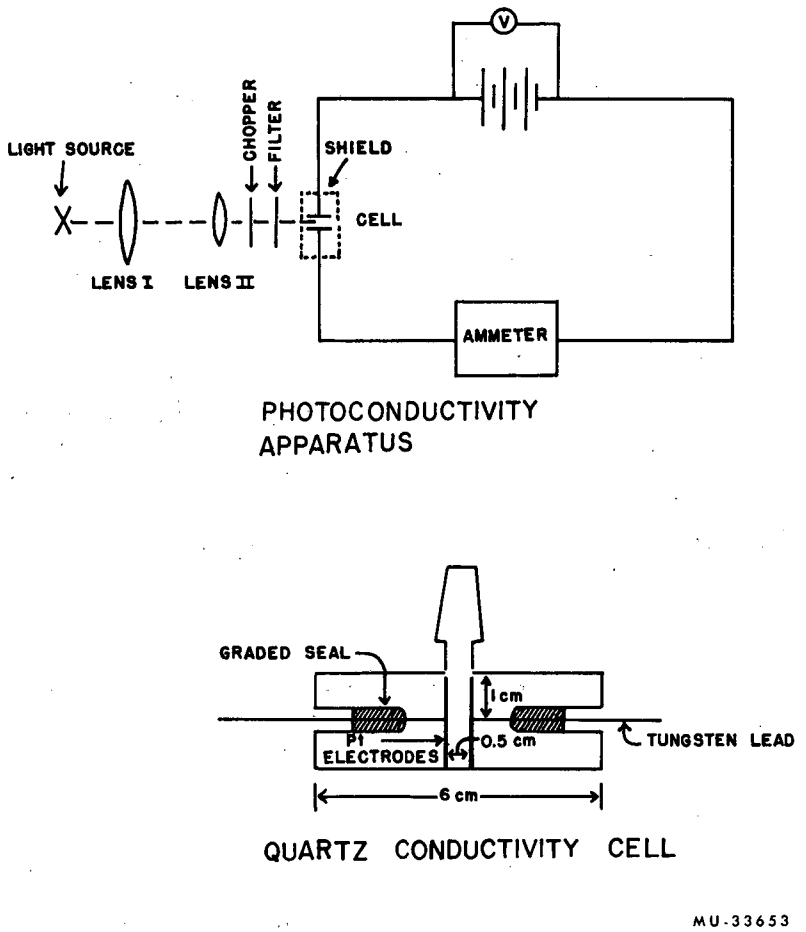

Fig. V-15. Photoconductivity apparatus. a. Block diagram of the measuring device. b. Conductivity cell (metal shielding is not shown).

e = the charge on the electron,

μ_n = the mobility of the negative charge carriers,

μ_p = the mobility of the positive charge carriers.

The mobility is defined as $\mu = v/\mathcal{E}$, the ratio of the velocity, v, of the carrier to the applied field, .

The conductivity is, then, the rate of transport of charge carriers through a unit square of the solution.

In explaining the data obtained, several assumptions were made:

(1) Each carrier bears unit charge.

(2) The mobility of the charge carriers is independent of the concentration of carriers. This implies that the conductivity should be directly proportional to the concentration of charge carriers.

(3) The conductivity is ionic and for each TCNE negative ion produced, a THF positive ion is produced as well.

3. Calculation of Ionic Velocities from Experimental Data

One form of Ohm's Law is

$$j = \sigma\mathcal{E}, \qquad \text{(V.20)}$$

where

j = the current density (amps/cm^2),

σ = the conductivity (ohm^{-1} cm^{-1}),

$\mathcal{E}$ = the electric field strength (volts/cm).

The current density is also given by

$$j = nev_n + pev_p, \qquad \text{(V.21)}$$

where

v_n = the velocity of the negative charge carrier,

v_p = the velocity of the positive charge carrier.

Assume that $n = p$ and that $v_n \sim v_p$.

Then,

$$v = \frac{\sigma \mathcal{E}}{2ne} \tag{V.22}$$

From the EPR data, the concentration of negative ions, n, is found to be $2.5 \times 10^{15}/cm^3$. Bearing in mind that the light intensity was a factor of 5 lower for the EPR than for the conductivity, and that the concentration goes as the square root of the light intensity, the concentration of negative carriers is approximately 5.75×10^{15} for the case of the conductivity. This result neglects the differences in the geometry of the cells for the two measurements.

Using Equation (V.22) and $n = 5.75 \times 10^{15}$ carriers/cm^3, $\mathcal{E} = 0.18$ volts/cm, and $\sigma = 2.33 \times 10^{-6}$ ohm^{-1} cm^{-1}, the results

$v = 5 \times 10^{-5}$ cm/sec or $\mu = 2.7 \times 10^{-4}$ cm^2/volt sec.

4. Calculation of the Ionic Velocities from Stokes' Law

By equating the electrostatic attractive force exerted by a field on a charged sphere to the retarding force due to the viscosity of the medium, we obtain

$$eE = 6\pi\eta\, a\, v, \tag{V.23}$$

where

η = the intrinsic viscosity of THF = 0.0107 Stokes (55,56) at 25° C,

a = the ionic radius of the carrier, estimated at 3.20 Å,

$e = 6 \times 10^{-10}$ esu, the charge on the electron,

v = the ionic velocity, and

E = the electric field in statvolts/cm = $300\mathcal{E}$.

Substituting the above values into Equation (V.23), we obtain

$$\frac{6 \times 10^{-10}}{(300)\ 6\pi(0.01)(3.20 \times 10^{-6})} = \frac{1}{3.2\pi(300)} = \frac{v}{\mathcal{E}},$$

$$v = \frac{\mathcal{E}}{3.2\pi(300)} = 6.5 \times 10^{-5} \text{ cm/sec},$$

or

$$\mu = 3.3 \times 10^{-4} \text{ cm}^2\text{/volt sec.}$$

5. Experimental Technique

The photoconductivity apparatus is diagrammed in Figure V-8. The direct current resistance was measured by applying a fixed voltage to the sample and simultaneously measuring the current flow by means of a picoammeter. The voltage supply consisted of a 90-volt direct current source in series with a variable resistance, so that the applied potential could be varied from 0 to 90 volts. In almost all cases the applied potential was less than one volt. In this region the current-voltage characteristic was linear (Fig. V-16). A General Radio Type 1809-A vacuum tube voltmeter was used for potential measurements. The picoammeter was a Keithley Model 410. The 0 to 63% rise time for the 10^{-7} amp scale was 0.001 sec. However, the Sanborn Recorder used in conjunction with the picoammeter had a 0 to 100% rise time of 0.01 sec. All effects observed occurred in times longer than these instrumental limitations. The light source was a Westinghouse H33-1-CD 400-watt mercury lamp that had been silvered except for a small region. Two glass lenses were used to focus the lamp onto the conductivity cell. They effectively cut off wavelengths shorter than 3100 Å. The cell itself was made entirely of quartz. The electrodes were platinum discs one cm in radius and 1/2 cm apart. The electrodes were masked to keep the light from hitting them directly, although the entire region between the plates was irradiated.

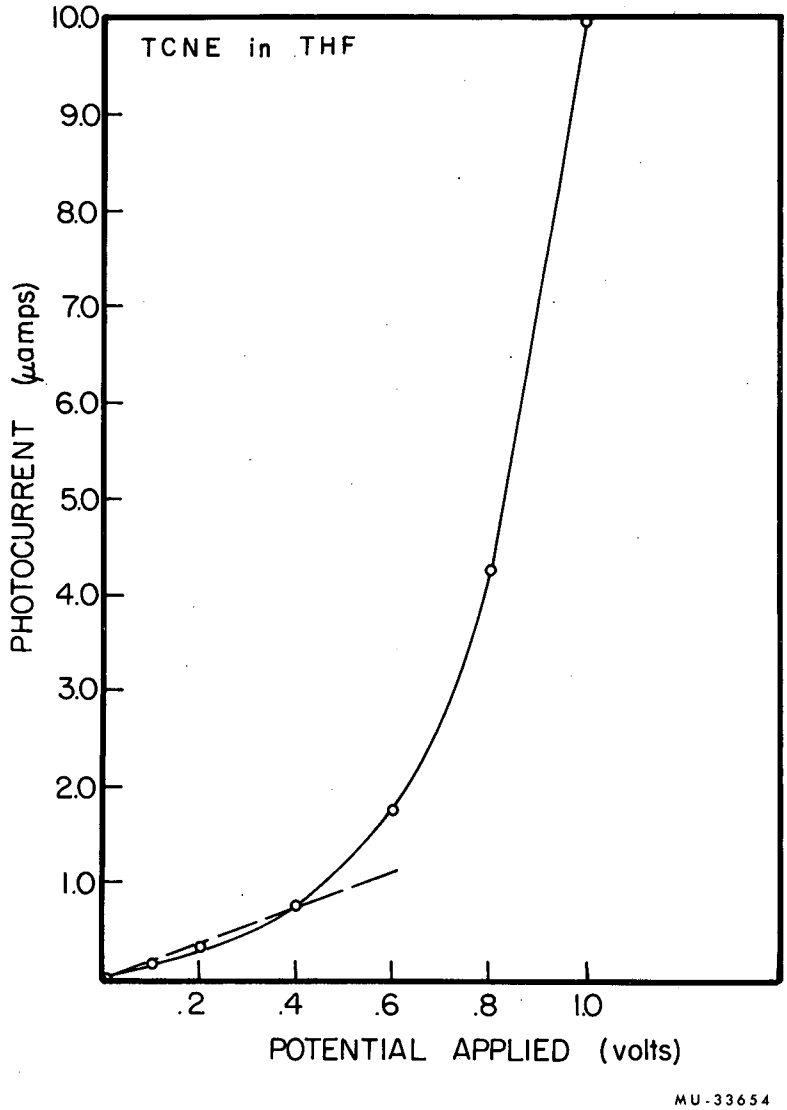

Fig. V-16. Maximum photocurrent for 0.01 M TCNE in THF as a function of the applied voltage.

6. Materials

Eastman Kodak TCNE was used. Eastman White Label THF was treated with solid KOH and then distilled from lithium aluminum hydride, as in the case of the EPR samples. The THF alone showed no conductivity changes when irradiated. The electrodes were cleaned with dilute sulfuric acid, ethanol, and distilled water. If the electrodes were not cleaned for several days, a back potential developed. The light intensity was compared with the light intensity for the EPR studies by using a photodiode. A factor of 5 decrease in intensity was observed for the EPR compared to the conductivity.

D. A Summary of EPR and Photoconductivity Results for the TCNE-THF System

Photoinduced electron paramagnetic resonance signals have been observed in a solution of 0.01 M TCNE in THF. Photoconductivity has been seen as well. The effective absorption for both phenomena occurs in the charge-transfer band of the complex (3100 Å to 4500 Å). The steady-state level for both the EPR and the photoconductivity is dependent upon the square root of the light intensity. Both effects showed second order decay kinetics. The growth curves for both phenomena can be explained by the rate equation

$$dn/dt + k_6 n^2 - \alpha L(1 - e^{-\beta t}) = 0, \quad (V.13)$$

where

α, β, and k_6 are constants,

L = a constant proportional to the light intensity,

n = the concentration of TCNE,

which predicts a square law initial rise, followed by a hyperbolic tangential rise. The equation also explains the steady state and the decay behavior.

The hyperfine splitting of the EPR spectrum shows the TCNE negative ion radical to be present. This same species and the THF positive ion radical are assumed to be responsible for the photoconductivity. The ionic velocities as calculated from Stokes' Law and from the conductivity measurements agree within approximately 20%. The differences in the geometry of the conductivity cell and the EPR tube made direct comparisons of the intensities of the two systems difficult.

SUMMARY

This work consists of studies of the movement of electrons within and between organic molecules. It was motivated by the interest which is now being shown in relating electronic motion in molecules to fundamental life processes. Complexes formed between molecules capable of donating and accepting electrons were studied as models for biological systems. Photoinduced and thermally-induced changes in the electrical, magnetic, and optical properties of these complexes, both solutions and solids, gave information concerning charge separation and charge transport phenomena in organic systems.

First, the dichroism of the optical absorption of solid complexes was studied. The charge-transfer absorption in the crystalline complex formed between coronene and p-chloranil was found to maximize when the scanning light was polarized parallel to the needle of the crystal. When the light was polarized perpendicular to the needle axis, the absorption in the charge-transfer region was essentially zero. These results indicated that the transition moment for the charge-transfer absorption was polarized parallel to the needle axis of the crystal--that is, along the line of centers joining the molecules. Both photoinduced and thermally-induced electron paramagnetic resonance (EPR) signals have been observed in the coronene-chloranil complex. These signals were explained by assuming that heat and light introduced paramagnetic imperfections in the crystals. Attempts were made to correlate thermally-induced EPR signals with thermally-induced conductivity changes in perylene-o-chloranil solid complex. No simple relationship between the two phenomena was found.

A general search was made for photoinduced EPR signals in liquid

complexes. Several systems were found which showed EPR photosignals with rise times and decay times of the order of milliseconds. One of the systems, p-chloranil dissolved in dioxane, was studied in detail. The system, however, showed various side reactions which made the interpretation of the data difficult. Since the free radical observed showed no hyperfine structure, the radical could not be identified from the EPR signal.

The TCNE-THF complex was relatively more stable, showed longer rise and decay times, and the photoinduced paramagnetic species was positively identified by the hyperfine splitting of the EPR spectrum to be TCNE negative ion radical. It was a relatively long-lived species, having a half-life of approximately 20 sec. Photoconductivity was seen in the TCNE-THF complex as well. The kinetics for the photoconductivity agreed well with the kinetics for the EPR. This was because the TCNE negative ion radical served the dual function of an ion and a radical and could be detected either by its paramagnetism or by the fact that it contributed to the conductivity of the solution. A kinetic rate law was proposed which satisfactorily fit both the photoinduced EPR and the photoconductivity data.

These results seemed to indicate that the system, TCNE dissolved in THF, is, in fact, a system where the reversible transfer of an electron from an organic electron donor molecule to an organic electron acceptor molecule in solution can be produced by light. Such a photoinduced electron transfer may well be of importance in biological systems.

ACKNOWLEDGMENTS

I wish to express my appreciation to Professor Melvin Calvin, who showed that one ought to suit the method to the problem, rather than the problem to the method. His advice, his criticism, and his acting rather as a Socratic gadfly have led to a more meaningful result.

To Professor M. Kronenberg of the University of Leiden, and to Professors K. Sauer and R. Ruby of the University of California at Berkeley, I give my thanks. Without their help the experimental work would have been much more limited. Thanks, also, to Drs. R. Foss and D. Baker for many varied and interesting discussions.

The Lawrence Radiation Laboratory personnel were always helpful concerning problems of instrumentation.

To the National Institutes of Health I owe a great deal for the fellowship support they provided over the tortuous course of the last four years.

This work was supported, in part, by the United States Atomic Energy Commission.

TABLE OF MATERIALS

DONOR

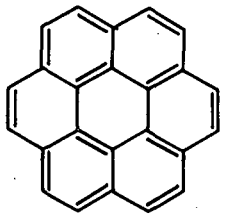

Coronene

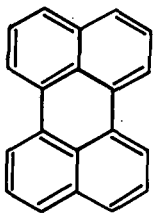

Perylene

Tetrahydrofuran

ACCEPTOR

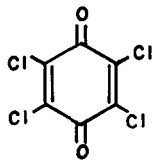

p-chloranil

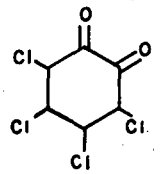

o-chloranil

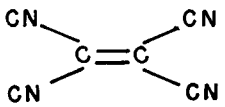

Tetracyanoethylene

MU-33655

APPENDIX I

BIBLIOGRAPHY

1. M. Calvin, Angew. Chem. 68, 253 (1956).

2. M. Calvin, "Some Photochemical and Photophysical Reactions of Chlorophyll and Its Relatives," University of California Radiation Laboratory Report UCRL-9170 (1960).

3. A. Szent-Györgyi, An Introduction to Submolecular Biology (Academic Press, New York, 1960).

4. G. Tollin, P. D. Sogo, and M. Calvin, in Photoperiodism and Related Phenomena in Plants and Animals (Am. Assn. for Adv. of Science, Washington, D. C., 1959), p. 47.

5. D. Kearns, Thesis, University of California, Berkeley (1960), University of California Radiation Laboratory Report UCRL-9120, March 1960.

6. D. Kearns, G. Tollin, and M. Calvin, J. Chem. Phys. 32, 1020 (1960).

7. J. W. Eastman, Thesis, University of California, Berkeley (1961), University of California Radiation Laboratory Report UCRL-9722, August 1961.

8. J. W. Eastman, G. Engelsma, and M. Calvin, J. Am. Chem. Soc. 84, 1339 (1962).

9. R. S. Mulliken, J. Phys. Chem. 56, 801 (1952).

10. R. S. Mulliken, J. Am. Chem. Soc. 74, 811 (1952).

11. R. S. Mulliken, J. Chem. Phys. 19, 514 (1951).

12. F. Wöhler, Pharmaceutisches Central Blatt (now Chemisches Zentralblatt), 39, 611 (1844).

13. A. Kekulé, Lehrbuch der Organischen Chemie (F. Enke, Erlangen, 1866), Vol. III, p. 97.

14. P. Pfeiffer, Organische Molekülverbindungen (F. Enke, Stuttgart, 1921).

15. P. Pfeiffer, Organische Molekülverbindungen, 2nd Ed. (F. Enke, Stuttgart, 1927).

16. E. Weitz, Z. Elektrochem. 34, 538 (1928).

17. H. A. Benesi and J. H. Hildebrand, J. Am. Chem. Soc. 71, 2703 (1949).

18. W. Brackman, Rec. trav. chim. 68, 147 (1949).

19. S. F. Mason, Quart. Rev. (London) 15, 287 (1961).

20. S. P. McGlynn, Chem. Rev. 58, 1113 (1958).

21. J. N. Murrell, Quart. Rev. (London) 15, 191 (1961).

22. G. Junghähnel, in Theory and Structure of Complex Compounds, B. Jezowska-Trzebiatowska, Ed. (Pergamon Press, Oxford, London, New York, 1963).

23. G. Briegleb, Elektronen-Donator-Acceptor-Komplexe (Springer-Verlag, Berlin-Gottingen-Heidelberg, 1961).

24. H. Hansen, Acta. Cryst. 16, 1147 (1963).

25. J. Anderson, Nature 140, 583 (1937).

26. K. Nakamoto, J. Am. Chem. Soc. 74, 1739 (1952).

27. B. G. Anex and L. J. Parkhurst, ibid. 85, 3302 (1963).

28. J. M. Robertson and J. G. White, J. Chem. Soc. (London) 1945, 607.

29. R. S. Mulliken, J. Am. Chem. Soc. 74, 814 (1952).

30. R. Tsuchida and M. Kobayashi, Bull. Chem. Soc. Japan 13, 619 (1938).

31. H. Akamatu, H. Inokuchi, and Y. Matsunaga, Nature 173, 168 (1954).

32. H. Kainer, D. Bijl, and A. C. Rose-Innes, Naturwiss. 41, 313 (1954).

33. J. W. Eastman, G. Androes, and M. Calvin, J. Chem. Phys. 36, 1197 (1962).

34. H. Inokuchi and H. Akamatu, "Electrical Conductivity of Organic Semiconductors," in Solid State Physics Advances and Research Applications, Vol. XII, F. Seitz and D. Trumbull, Ed. (Academic Press, New York, London, 1961).

35. D. Kearns, Thesis, University of California, Berkeley (1960), University of California Radiation Laboratory Report UCRL-9120, March 1960.

36. C. Lagercrantz and M. Yhland, Acta Chem. Scand. 16, 1043 (1962).

37. C. Lagercrantz and M. Yhland, ibid. 16, 1799 (1962).

38. C. Lagercrantz and M. Yhland, ibid. 16, 1807 (1962).

39. G. O. Schenck, Z. Elektrochem., Ber. Bunsenges. physik. Chem. 64, 997 (1960).

40. A. Schönberg, Präparative Organische Photochemie (Springer-Verlag, Berlin-Göttingen-Heidelberg, 1958).

41. M. R. Klein and G. W. Barton, Jr., Rev. Sci. Inst. 34, 754 (1963).

42. T. L. Cairns, et al., J. Am. Chem. Soc. 80, 2775 (1958).

43. R. E. Merrifield and W. D. Phillips, ibid. 80, 2778 (1958).

44. R. Vars, L. A. Tripp, and L. W. Pickett, J. Phys. Chem. 66, 1754 (1963).

45. R. Ward, J. Chem. Phys. 38, 853 (1963).

46. W. D. Phillips, J. C. Rowell, and S. J. Weissman, ibid. 33, 626 (1960).

47. E. Kamke, Differential Gleichungen, 2nd Ed. (Akademische Verlagsgesellschaft, Becker and Erler, Rome-Leipzig, 1943), Vol. I, p. 21.

48. D. J. Ingram, Free Radicals as Studied by Electron Spin Resonance (Butterworths Scientific Publications, London, 1958).

49. A. Carrington, Quart. Rev. (London) 17, 67 (1963).

50. G. M. Androes and M. Calvin, "Electron Paramagnetic Resonance in Biology," University of California Radiation Laboratory Report UCRL-9823 (1961).

51. G. E. Pake, Paramagnetic Resonance (W. A. Benjamin, Inc., New York, 1961).

52. R. B. Withrow and A. P. Withrow, in Radiation Biology, A. Hollaender, Ed. (McGraw-Hill, New York, London, Toronto, 1956), Vol. III, p. 173.

53. R. H. Bube, Photoconductivity of Solids (Wiley, New York, 1960).

54. H. Meier, Die Photochemie der Organischen Farbstoffe (Springer-Verlag, Berlin-Göttingen-Heidelberg, 1963).

55. International Critical Tables (McGraw-Hill, New York and London, 1930), Vol. VII, p. 216.

56. F. Thole, J. Chem. Soc. (London) 105, 2004 (1914).

This report was prepared as an account of Government sponsored work. Neither the United States, nor the Commission, nor any person acting on behalf of the Commission:

A. Makes any warranty or representation, expressed or implied, with respect to the accuracy, completeness, or usefulness of the information contained in this report, or that the use of any information, apparatus, method, or process disclosed in this report may not infringe privately owned rights; or

B. Assumes any liabilities with respect to the use of, or for damages resulting from the use of any information, apparatus, method, or process disclosed in this report.

As used in the above, "person acting on behalf of the Commission" includes any employee or contractor of the Commission, or employee of such contractor, to the extent that such employee or contractor of the Commission, or employee of such contractor prepares, disseminates, or provides access to, any information pursuant to his employment or contract with the Commission, or his employment with such contractor.